Human TDP1, APE1 and TREX1 repair 3′-DNA–peptide/protein cross-links arising from abasic sites *in vitro*

Xiaoying Wei[1,2,†], Zhishuo Wang[1,†], Caroline Hinson[3] and Kun Yang [1,*]

[1]Division of Chemical Biology and Medicinal Chemistry, College of Pharmacy, The University of Texas at Austin, Austin, TX 78712, USA, [2]Department of Molecular Biosciences, The University of Texas at Austin, Austin, TX 78712, USA and [3]Department of Chemistry, The University of Texas at Austin, Austin, TX 78712, USA

ABSTRACT

Histones and many other proteins react with abundant endogenous DNA lesions, apurinic/apyrimidinic (abasic, AP) sites and/or 3′-phospho-α,β-unsaturated aldehyde (3′-PUA), to form unstable but long-lived Schiff base DNA–protein cross-links at 3′-DNA termini (3′-PUA–protein DPCs). Poly (ADP-ribose) polymerase 1 (PARP1) cross-links to the AP site in a similar manner but the Schiff base is reduced by PARP1's intrinsic redox capacity, yielding a stable 3′-PUA–PARP1 DPC. Eradicating these DPCs is critical for maintaining the genome integrity because 3′-hydroxyl is required for DNA synthesis and ligation. But how they are repaired is not well understood. Herein, we chemically synthesized 3′-PUA-aminooxylysine-peptide adducts that closely resemble the proteolytic 3′-PUA–protein DPCs, and found that they can be repaired by human tyrosyl-DNA phosphodiesterase 1 (TDP1), AP endonuclease 1 (APE1) and three-prime repair exonuclease 1 (TREX1). We characterized these novel repair pathways by measuring the kinetic constants and determining the effect of cross-linked peptide length, flanking DNA structure, and the opposite nucleobase. We further found that these nucleases can directly repair 3′-PUA–histone DPCs, but not 3′-PUA–PARP1 DPCs unless proteolysis occurs initially. Collectively, we demonstrated that *in vitro* 3′-PUA–protein DPCs can be repaired by TDP1, APE1, and TREX1 following proteolysis, but the proteolysis is not absolutely required for smaller DPCs.

INTRODUCTION

An apurinic/apyrimidinic (abasic, AP, Scheme 1) site is one of the most abundant DNA lesions. It is produced from the spontaneous or enzymatic hydrolysis of a nucleotide's glycosidic bond with a frequency of ∼10,000 times per cell per day under typical conditions (1). Such number increases dramatically after the exposure of DNA to alkylating agents or reactive oxygen species (2,3). The AP site inhibits the DNA replication and transcription (4,5). It can be bypassed by translesion DNA synthesis polymerases in a highly error-prone manner and is primarily repaired by base excision repair (6,7). The AP site is unstable and can undergo spontaneous β-elimination to yield a single-strand break bearing a 3′-phospho-α,β-unsaturated aldehyde (3′-PUA, Scheme 1). This process is slow under physiological temperature and pH but can be greatly accelerated by AP lyases (8,9), polyamines (10–12), nucleophilic peptides (13–15), histones (16,17) and other proteins, such as mitochondrial transcription factor A (18). The steady-level of 3′-PUA in human embryonic kidney 293T cells can be as high as ∼13,000 per genome (19). Numerous studies have demonstrated that both AP sites and 3′-PUA can react with nucleobase amines and protein nucleophiles (e.g. lysine and cysteine residues) to yield various types of more deleterious DNA-DNA cross-links (20–22) and DNA–protein cross-links (DPCs) (16,17,23–40), respectively. These adducts, if unrepaired, will block DNA replication and greatly threaten the genome integrity.

Approximately 145 bp of DNA wraps around a histone octamer consisting of two copies of H2A, H2B, H3 and H4 to form a nucleosome core particle (NCP), the basic unit of chromatin (41). Independently synthesizing a NCP containing a site-specific AP site at nearly ten super-helix locations (SHL), Greenberg *et al.* revealed a general phenomenon that, similar to AP lyases, the histone lysine residue reacts with the AP site to form a Schiff base AP-histone DPC followed by β-elimination, yielding a 3′-phospho-α,β-

---
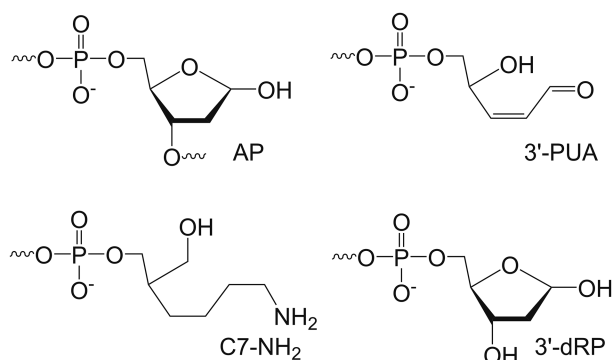
**Scheme 1.** Structure of AP, 3′-PUA, C7-NH$_2$ and 3′-dRP.

unsaturated aldehyde-histone cross-link (3′-PUA–histone DPC, Scheme 2) (16,17,42–45). Unlike the 3′-PUA-AP lyase adduct that is often transient, the hydrolysis of 3′-PUA–histone DPCs to yield 3′-PUA is slow, resulting in persistent DPCs. For example, when the AP site was installed at position 89 (SHL 1.5) in the NCP, a hot-spot for DNA damage (46,47), the yield of 3′-PUA–histone DPC reached a plateau (∼20%) following 8-h incubation at 37°C and stayed the same after an additional 16-h incubation (17). Schiff base 3′-PUA–histone DPCs can be detected and further isolated by sodium dodecyl sulfate-polyacrylamide gel electrophoresis (SDS-PAGE) without prior stabilization by NaBH$_4$ (48). The isolated 3′-PUA–histone DPCs have half-lives of 10–14 h under physiological pH and temperature (see below).

Many other non-histone proteins such as glyceraldehyde-3-phosphate dehydrogenase (GAPDH) (30), X-ray repair cross-complementing protein 1 (XRCC1) (25), and Poly (ADP-ribose) polymerase 2 (PARP2) (29) have been demonstrated to react with AP sites and/or 3′-PUA to form 3′-PUA–protein DPCs. GAPDH and XRCC1 were also found to cross-link preferentially to 3′-PUA as compared to the AP site (25,30). Some bifunctional DNA glycosylases, such as 8-oxoguanine DNA glycosylase 1 (OGG1), tightly bind to the AP site (49). This has been proposed to sequester the base excision repair intermediates prior to the completion of the repair, but it may also provide the opportunity to form a long-lived, covalent 3′-PUA-OGG1 DPC (40,50), The formation of these DPCs has been mainly demonstrated by reacting the AP site or 3′-PUA-containing DNA with recombinantly purified proteins and/or cell lysates. The OGG1-DPC was also observed in mammalian cells after DNA methylating agent treatment through a rapid approach to DNA adduct recovery (RADAR) assay (51). Similar to 3′-PUA–histone DPCs, these non-histone Schiff base 3′-PUA–protein DPCs are also unstable but long-lived based on the observations that they can be detected by SDS-PAGE without prior NaBH$_4$ stabilization and/or little DPC decomposition was observed after incubating with an excess amount of competitor DNA for several hours at 37°C. Unlike 3′-PUA–histone DPCs that are considered as DNA lesions, the formation of the 3′-PUA-XRCC1 DPC was hypothesized to warrant the accurate repair of AP sites and 3′-PUA through temporal protection of the lesions and re-

cruitment of the downstream base excision repair enzymes (25). Regardless of their biological significance, these long-lived Schiff base 3′-PUA–protein DPCs must be promptly removed because 3′-hydroxyl (3′-OH) is required for DNA synthesis and strand ligation. However, how they are repaired is unclear.

PARP1 is an abundant chromatin-associated nuclear enzyme that plays important roles in DNA damage recognition and repair. Upon binding to DNA lesions, PARP1 is activated for Poly (ADP-ribose) synthesis which recruits the downstream DNA repair enzymes (52). It has been found that PARP1 has weak AP lyase activity (27). It reacts with the AP site to form a Schiff base DPC followed by β-elimination to yield a 3′-PUA–PARP1 DPC (Scheme 2) (28,53). Different from 3′-PUA–histone DPCs, the 3′-PUA–PARP1 DPC is stable, which is ascribed to the Schiff base reduction through PARP1's intrinsic redox ability (28,53). Formation of 3′-PUA–PARP1 DPCs was first demonstrated *in vitro* with a purified enzyme and AP site-containing DNA. Using the DNA fiber-spread analysis and RADAR assay, Wilson *et al.* further verified the 3′-PUA–PARP1 DPC formation in mouse embryonic fibroblasts following methyl methanesulfonate treatment in which the base excision repair was overwhelmed (28,53). And the DPC amount increased after an additional treatment by 4-amino-1,8-naphthalimide, a PARP1 inhibitor. These observations led to the speculation that 3′-PUA–PARP1 DPC formation can partially be the cytotoxic source of DNA methylating and PARP1 inhibitor drugs. Thus, it is of great importance to understand how this type of DPC is repaired. Wilson *et al.* have demonstrated that 3′-PUA–PARP1 DPC cannot be directly repaired by both tyrosyl-DNA phosphodiesterase 1 (TDP1) and AP endonuclease 1 (APE1) likely due to the bulky size (28,53). Based on this, they speculated that cellular 3′-PUA–PARP1 DPC repair may involve proteolysis. Indeed, they subsequently demonstrated that 3′-PUA–PARP1 DPC is polyubiquitinated and degraded by the proteasome (53). Pommier *et al.* recently found that 3′-PUA–PARP1 DPC can also be degraded by a DNA-dependent metalloprotease, Spartan (54). However, how the remaining 3′-PUA–PARP1 peptide adducts following proteolysis that still prevent the DNA synthesis and strand ligation are eradicated is incompletely understood. Using a model substrate (C7-NH$_2$, Scheme 1) that mimics the proteolyzed 3′-PUA–PARP1 DPC, Wilson *et al.* demonstrated *in vitro* that TDP1, but not APE1, removed the adduct in an enzyme concentration-dependent manner (53). However, this model substrate differs significantly from the physiological one by both the linkage and size. And it remains elusive whether any other 3′-PUA-peptide adduct repair enzyme(s) exists.

In this work, we first developed a chemical approach to synthesize stable and site-specific 3′-PUA–protein DPC analogues (3′-PUA–OxyLys–peptides) through oxime ligation by reacting 3′-PUA with aminooxylysine (OxyLys)-containing peptides. *In vitro* reconstitution experiments using 3′-PUA–OxyLys–peptides as substrates identified three enzymes, TDP1, APE1, and three-prime repair exonuclease 1 (TREX1), that were able to remove 3′-PUA–OxyLys–peptides. Kinetic studies using 3′-PUA–OxyLys–
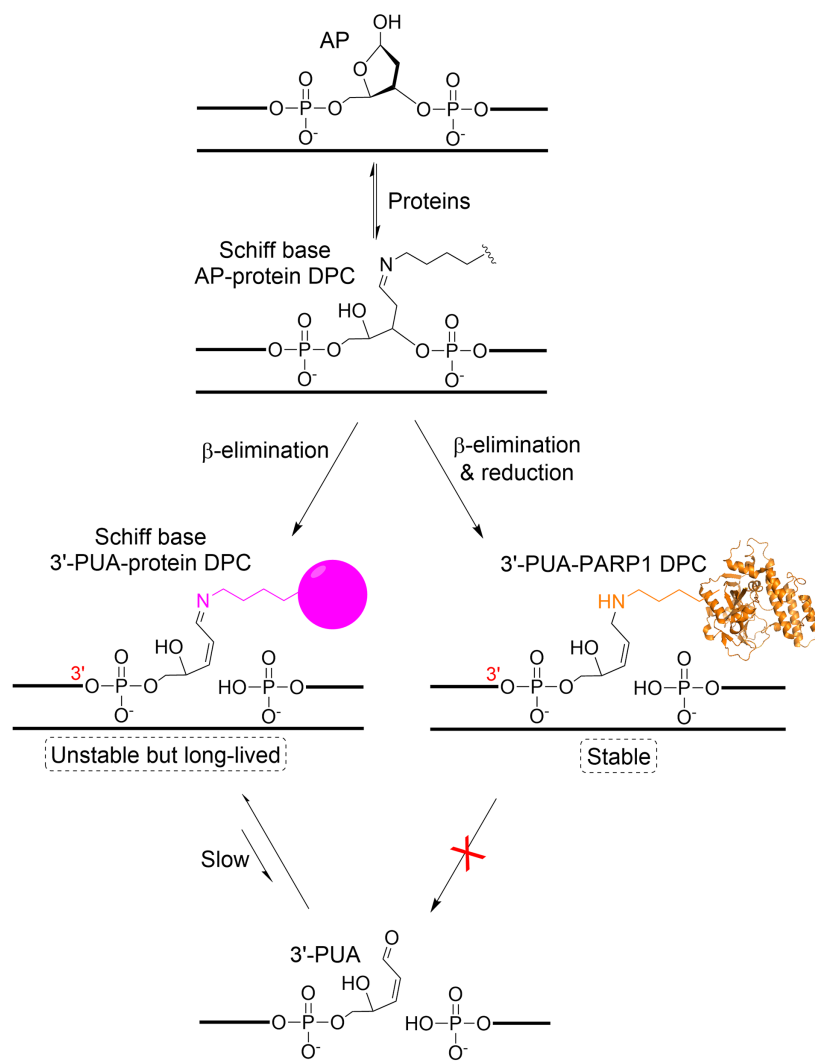
Scheme 2. Mechanistic formation of 3′-PUA–protein DPCs.

peptide$_{10mer}$ within nicked DNA as a substrate demonstrated that the adduct removal efficiency of APE1 is 1.8-fold higher than TDP1. While TDP1 has no preference for the flanking DNA structure, APE1 removes the adduct only within the nick and 5′-overhangs, and TREX1 slightly prefers the blunt end, 3′- and 5′-overhangs to the nicked DNA. Additionally, TDP1 and APE1 have no preference for the opposite nucleobase, but TREX1 removes the adduct slightly (1.3–1.5-fold) more efficiently when a pyrimidine base (T and C) is opposite. Notably, we further demonstrated that all three nucleases were able to remove the 3′-PUA–histone DPC with moderate efficiency. Finally, we found that all these nucleases failed to remove 3′-PUA–PARP1 DPC unless the DPC is pre-treated by proteinase K. Taken all together, we demonstrated for the first time that *in vitro* coupled with proteolysis, 3′-PUA–protein DPCs can be redundantly and complementarily repaired by TDP1, APE1, and TREX1. It should be noted that proteolysis is not absolutely required for smaller DPCs, such as 3′-PUA–histone DPCs.

## MATERIALS AND METHODS

Materials and general methods

All oligos were purchased from Integrated DNA Technologies and purified by 20% urea–PAGE. Uracil-DNA glycosylase (UDG, Cat. # M0280S), T4 polynucleotide kinase (T4 PNK, Cat. # M0201S), proteinase K (Cat. # P8107S), Phusion® high-fidelity DNA polymerase (Cat. # M0530S), Quick Ligation™ Kit (Cat. # M2200S), Human APE1 (Cat. # M0282S) and exonuclease III (Ex-oIII, Cat. # M0206S) were purchased from the New England Biolabs. Human DNA polymerase epsilon (Polε) was purchased from Enzymax (Lexington, KY). Human Werner syndrome protein (WRN) was kindly provided by Professor Vilhelm Bohr (National Institutes of Health, USA). Human Mre11-Rad50-Nbs1 (MRN) was obtained from Professors Ilya Finkelstein and Tanya Paull (The University of Texas at Austin). Human DNA polymerase delta (Polδ) was shared by Professor Mark Hedglin (The Pennsylvania State University). Chemicals were pur-

chased from Sigma-Aldrich, Fisher Scientific™, and Chem-Impex International. C18 Sep-Pak desalting columns (Cat. #: WAT020515) were purchased from Waters. The 6-carboxyfluorescein (6-FAM)-containing oligos were visualized by a Typhoon 9400 Imager and quantified by Image-QuantTL. The molecular weights of modified oligos were determined by matrix-assisted laser desorption/ionization-time-of-flight (MALDI-TOF) mass spectrometer using 3-hydroxypicolinic acid as the matrix. The plots were generated and the statistical analysis was carried out using GraphPad Prism 6.0. Nuclear magnetic resonance (NMR) spectra were collected on an Agilent 400-MR spectrometer. The ^{1}H NMR (400 MHz) chemical shifts were determined relative to deuterium water (D_2O) as the internal reference (D_2O: $\delta = 4.79$ ppm). The ^{13}C NMR (100 MHz) chemical shifts were determined in D_2O. High-resolution mass spectra (HRMS) were obtained with an Agilent Technologies 6530 Accurate-Mass Q-TOF LC/MS (ESI).

Determining the stability of 3′-PUA–histone DPCs

Plasmids (pET3a-H2B, pET3a-H4) that express *Xenopus laevis* histone H2B and H4 were obtained from Professor Marc Greenberg (The Johns Hopkins University). H2B and H4 were purified following the reported procedures (41). To generate the AP site-containing oligo O5 (Table 1), a reaction (3 ml) containing an oligo with an internal 2′-deoxyuracil (dU, 60 nmol), 1x buffer (20 mM Tris–HCl, pH 8.0, 1 mM DTT, 1 mM EDTA) and UDG (300 units) was first incubated at 37°C for 1.5 h, followed by phenol–chloroform extraction (2 times) and ethanol precipitation (2 times). The precipitated DNA (45 nmol) was resuspended in H_2O and stored at -80°C. To prepare 3′-PUA–histone DPCs, a reaction mixture (1 ml) including oligo O5 (0.5 nmol) and histone H2B or H4 (5 nmol) in a HEPES buffer (10 mM, pH 7.5) was incubated at 37°C for 19 h, followed by addition of SDS to a final percentage of 0.1% and concentrating at 16°C using a 3.0 kDa cut-off Amicon centrifugal filter. The concentrated sample (∼50 μl) was mixed with an equal volume of loading buffer (25 mM HEPES, pH 7.5, 40% glycerol, 0.2% SDS) and analyzed by 15% SDS-PAGE. The gel (12 × 8 × 0.15 cm) was run at 4°C until the bromophenol blue migrated to the middle. The DPC bands were cut, smashed, mixed with an eluting buffer (2 ml, 0.2 M NaCl, 1 mM EDTA, 0.1% SDS), and rotated at 4°C overnight. Following centrifugation, the supernatant was taken out, concentrated, and exchanged (6 times, 10-fold dilution/time) to a HEPES buffer (10 mM, pH 7.5) at 4°C. The isolated DPCs were incubated at 37°C. An aliquot was taken out at different time points (0–56 h), stored at –80°C, and finally analyzed by 15% SDS-PAGE at 4°C as described above.

Synthesis of (*S*)-4-(aminooxy)-1-carboxybutan-1-aminium chloride (OxyLys-HCl)
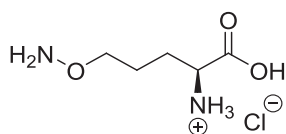
(*S*)-2-Amino-5-(((tert-butoxycarbonyl)amino)oxy) pentanoic acid was synthesized as previously descried (55,56). To remove the tert-butyloxycarbonyl group, a 5 ml microcentrifuge tube containing 6 N hydrochloride acid (HCl, 520 μl, 3.12 mmol), (*S*)-2-amino-5-(((tert-butoxycarbonyl)amino)oxy)pentanoic acid (0.1 mmol, 24.8 mg), methanol (2.0 ml) and water (2.0 ml) was vortexed at room temperature for 4 h. The solvent was removed under reduced pressure. The residue was dried under vacuum to obtain (*S*)-4-(aminooxy)-1-carboxybutan-1-aminium chloride as a gray solid (18.0 mg). ^{1}H NMR (D_2O, 400 MHz): δ (ppm) 4.11 (t, $J = 6.0$ Hz, 2H), 4.07 (t, $J = 6.4$ Hz, 1H), 2.10–1.96 (m, 2H), 1.91–1.77 (m, 2H). ^{13}C NMR (D_2O, 100 MHz): δ (ppm) 171.8, 74.1, 52.5, 26.1, 22.9. HRMS-ESI$^+$: calculated for $C_5H_{13}O_3N_2^+$, 149.0921; found 149.0920.

Synthesis of 3′-PUA-OxyLys and 3′-PUA–OxyLys–peptides

OxyLys containing peptides were synthesized through a standard solid-phase peptide synthesis (56). To prepare 3′-PUA, the AP site-containing oligo (21 nmol) was diluted into a sodium phosphate buffer (10 mM, pH 7.0) with a final concentration of 14 μM. The sample was then split into 50 μl/tube, heated at 95°C (lid temperature = 105°C) for 30 min, and then cooled down on ice. To generate 3′-PUA-OxyLys or 3′-PUA-OxyLys peptide cross-links, OxyLys or OxyLys-peptide was dissolved in H_2O, added to the heated AP site with a ratio of 1000:1 (OxyLys) or 100:1 (OxyLys-peptide), and neutralized (confirmed with pH paper) with addition of 1 M HEPES (pH 7.5). The reaction mixture was incubated at 37°C for 2–4 h, followed by concentrating down to ∼50 μl in a speed vacuum. The residue was then mixed with an equal volume of loading buffer (95% formamide, 25 mM EDTA) and loaded on a 20% urea–PAGE gel (18 × 16 × 0.8 cm). The gel was run at room temperature with a power limit of 15 W until the bromophenol blue migrated to the bottom. The desired band was cut, smashed, mixed with 3 ml eluting buffer (0.2 M NaCl, 1 mM EDTA), wrapped with aluminium foil, and rotated at room temperature overnight. The elute was spun down and the supernatant was carefully taken out and desalted with a C18 Sep-Pak cartridge. The 3′-PUA–OxyLys–peptide adduct (P1–P4, ∼2.5 nmol) was dissolved in water, characterized by MALDI-TOF mass spectrometry, and stored at –80°C.

Preparation of nicked DNA containing a 3′-PUA–OxyLys–peptide and a 5′-phosphate

Oligo O9 (Table 1) was prepared in a reaction (150 μl) containing the corresponding, unphosphorylated oligo (12 nmol), 1× T4 PNK buffer (70 mM Tris–HCl, pH 7.6, 10 mM $MgCl_2$, 5 mM DTT) and 1.3 mM ATP. The mixture was incubated at 37°C for 4 h, followed by phenol–chloroform extraction (two times) and ethanol precipitation (two times). The 5′-phosphorylated oligo (11.7 nmol) was resuspended in H_2O and the completed 5′-phosphorylation was confirmed by MALDI-TOF mass spectrometry. A reaction (60 μl) containing oligo O9 (2.25 nmol), oligo O7 (375 pmol), sodium phosphate (10 mM, pH 7.0) and NaCl

Table 1. Oligonucleotides and 3′-PUA–OxyLys–peptides used in this study. The AP site was prepared by treating the 2′-deoxyuracil (dU) with *E. coli* uracil–DNA glycosylase

Sample	Sequence (and notes)
O1	5′-6-FAM-CGAGATCTGAGTCCGG-3′ (3′-OH marker)
O2	5′-6-FAM-CGAGATCTGAGTCCGG-3′-P (3′-Phosphate marker)
O3	5′-ATTGAGCGGCCTCGGCACCGGGATTCTGAT-3′ (Competitor for reaction quenching)
O4	5′-GCACCGGGAT(AP)CTGAT-3′ (Supplementary Figure S4)
O5	5′-6-FAM-CGAGATCTGAGTCCGG(AP)AGCGCTAGCG-3′ (Prepare P1-P3, and 3′-PUA–histone DPCs)
O6	5′-6-FAM-ATCGCTTGCGCAGCGCTTGAGCTCGAGATCTGAGTCCGG(AP)AGCGCTAGCG-3′ (Prepare P4)
O7-8	5′-GTGAACCGTCAGATCCGCTAGCGCT̲ACCGGACTCAGATCTCG-3′ (3′-OH for O7, 3′-P for O8)
O9-10	5′-P-AGCGCTAGCGGATCTGACGGTTCAC-3′ (3′-OH for O9, 3′-P for O10)
O11-12	5′-GCGCTACCGGACTCAGATCTCG-3′ (3′-OH for O11, 3′-P for O12)
O13-14	5′-CGCTAGCGCTACCGGACTCAGATCTCG-3′ (3′-OH for O13, 3′-P for O14)
O15-16	5′-ACCGGACTCAGATCTCG-3′ (3′-OH for O15, 3′-P for O16)
O17-18	5′-ACTCAGATCTCGAGCTCAAGCGCTGCGCAAGCGAT-3′ (3′-OH for O17, 3′-P for O18)
O19-20	5′-GATCTCGAGCTCAAGCGCTGCGCAAGCGAT-3′ (3′-OH for O19, 3′-P for O20)
O21-22	5′-CGCTGCGCAAGCGAT-3′ (3′-OH for O21, 3′-P for O22)
O23-24	5′-GTGAACCGTCAGATCCGCTAGCGCT̲TCCGGACTCAGATCTCG-3′ (3′-OH for O23, 3′-P for O24)
O25-26	5′-GTGAACCGTCAGATCCGCTAGCGCT̲GCCGGACTCAGATCTCG-3′ (3′-OH for O25, 3′-P for O26)
O27-28	5′-GTGAACCGTCAGATCCGCTAGCGCT̲CCCGGACTCAGATCTCG-3′ (3′-OH for O27, 3′-P for O28)
O29-30	5′-6-FAM-CGAGATCTGAGTCCGG(AP)A̲GCGCTAGCGGATCTGACGGTTCAC-3′ (3′-OH for O29, 3′-P for O30)
O31	5′-6-FAM-CGAGATCTGAGTCCGGT-3′ (Supplementary Figure S21)
P1	5′-6-FAM-CGAGATCTGAGTCCGG-3′-PUA-OxyLys
P2	5′-6-FAM-CGAGATCTGAGTCCGG-3′-PUA-(GGA-OxyLys-R)
P3	5′-6-FAM-CGAGATCTGAGTCCGG-3′-PUA-(SGRG-OxyLys-GGKGL)
P4	5′-6-FAM-ATCGCTTGCGCAGCGCTTGAGCTCGAGATCTGAGTCCGG-3′-PUA-(SGRG-OxyLys-GGKGL)

(100 mM) was heated at 90°C for 5 min and quickly cooled on ice. 3′-PUA–OxyLys–peptide adduct (P1–P3, 150 pmol) was added to the reaction and the whole mixture was heated at 70°C for 10 min followed by gradually cooling down to room temperature overnight. The hybridized sample was mixed with an equal volume of 40% glycerol and loaded on a 20% native PAGE gel. The gel (20 × 16 × 0.8 cm) was run at 4°C with a constant power (3 W) until the bromophenol blue migrated to the middle of the gel. The desired band was cut, smashed, mixed with 2 ml eluting buffer (10 mM sodium phosphate, 10 mM HEPES, pH 7.5, 100 mM NaCl), wrapped with aluminium foil, and rotated at 4°C overnight. After that, the sample was spun down and the supernatant was carefully taken out, concentrated, and exchanged extensively (4 times, 10-fold dilution/time) to the hybridization buffer (10 mM sodium phosphate, pH 7.0, 100 mM NaCl) using a 3 kDa cut-off Amicon centrifugal filter at 4°C. The integrity of the purified nicked DNA was confirmed by native PAGE as described above. To generate the nicked DNA substrates for three-prime repair exonuclease 1 (TREX1), oligos with 3′-phosphorylated termini (Table 1, O8 and O10) were used, which were synthesized by Integrated DNA Technologies.

Plasmid construction, protein expression and purification

To generate the recombinant full-length human TDP1, the cDNA (Cat: HG11419-UT) that encodes TDP1 was purchased from Sino Biological, PCR amplified (5′-CAGGTCGGCTAGCATGTCTCAGGAAGGCGATTATGGGAG-3′; 5′-GACCATGATTACGAACTCGAGCTCGGTACC-3′), cut with restriction enzymes (NheI and XhoI) and ligated to the restriction enzyme-digested pET28a vector (Novagen). The generated vector (pET28a-TDP1) was verified by Sanger DNA sequencing serviced by the University of Texas at Austin Core Facility. pET28a-TDP1 was transformed to BL21(DE3) cells and the transformed cells were plated on a LB-agarose plate containing 50 μg/ml kanamycin, followed by incubating at 37°C overnight. A single colony was picked and grown in 10 ml LB media containing the above antibiotic and 1% glucose at 37°C overnight before inoculating to 1 l LB media with 50 μg/ml kanamycin and 1% glucose. The cells were grown at 37°C until the OD reached 0.6 followed by protein induction via adding IPTG to a final concentration of 1.0 mM and incubating at 30°C for 2 h. After induction, the cells were harvested at 4°C by centrifugation. The cells (3.3 g) were resuspended in a lysis buffer (30 ml, 20 mM Tris–HCl, pH 7.9, 500 mM NaCl, 5 mM imidazole, 5 mM β-ME, 1 mM PMSF) and sonicated on ice. The cell lysate was centrifuged (4°C, 12 500 rpm, 30 min). The supernatant was collected, filtered with 0.45 μm nitrocellulose filter membrane, mixed with 1 ml cobalt resin, and rotated at 4°C for 1 h. The mixture was passed through a gravity column, the resin was washed extensively with the lysis buffer without PMSF. The protein was eluted out with a buffer (20 mM Tris–HCl, pH 7.9, 500 mM NaCl, 5 mM β-ME) containing increased concentrations of imidazole (50 mM-1 M). The eluted fractions were analyzed by 10% SDS-PAGE. The fractions containing pure TDP1 were combined, concentrated, and exchanged to a storage buffer (50 mM Tris–HCl, pH 7.5, 50 mM KCl, 1 mM EDTA, 2 mM DTT). The TDP1 concentration was determined by the Bradford assay. The protein (~12 mg per 1 l cells) was aliquoted, flash frozen with liquid N_2, and stored at –80°C.

To generate the catalytically inactive mutant TDP1 (H263A), the mutation was created by site-directed mutagenesis (5′-GGATATTGCGTTTGGAACAC ACGCCACGAAAATGATGCTGCTGCTC-3′; 5′-GAGCAGCAGCATCATTTTCGTGGCGTGTGTTC CAAACGCAATATCC-3′) using the cDNA (Sino Biological, Cat: HG11419-UT) as the template and confirmed by Sanger sequencing. The coding sequence for TDP1-H263A was amplified and subcloned into the pET-28a vector, and the protein expression and purification were performed as described above.

Plasmids (pLM303x-TREX1$_{1–242}$ and pLM303-TREX1$_{1–242}$ -D18N) that express the wild type (WT) and catalytically inactive mutant (D18N) TREX1 bearing residues 1–242 were generously provided by Professor Fred Perrino (Wake Forest School of Medicine). The cell culture and purification were performed as previously described (57) with some modifications. The pLM303x-TREX1$_{1–242}$ plasmid was transformed into Rosetta (DE3) cells, plated on a LB agarose plate containing 50 μg/ml kanamycin and 34 μg/ml chloramphenicol, followed by incubation overnight at 37°C. A single colony was picked, cultured in 20 ml LB media containing 50 μg/ml kanamycin and 34 μg/ml chloramphenicol overnight at 37°C before inoculating to 2 l LB media with the above antibiotics. The cells were cultured at 37°C with shaking (200 rpm) until the OD reached to 0.6. The cells were induced by IPTG (0.5 mM) and cultured overnight at 16°C. Half of the cells (∼2.5 g) were resuspended in a lysis buffer (30 ml, 20 mM Tris–HCl, pH 7.5, 200 mM NaCl, 1 mM EDTA, 5 mM β-ME, 0.1 mM PMSF) containing 1 tablet of EDTA-free Pierce™ protease inhibitor cocktail (ThermoFisher, Cat. # A32955) and sonicated, followed by centrifugation at 4°C. The supernatant was carefully collected, filtered with 0.45 μm nitrocellulose filter membrane, bound to the Amylose resin (1.5 ml, New England Biolabs, Cat. # E8021S), and incubated at 4°C for 1 h with gentle shaking. The mixture was passed through a gravity column at 4°C. The resin was washed extensively with the lysis buffer, followed by washing with an equilibrium buffer (50 mM Tris–HCl, pH 7.5, 100 mM NaCl, 10% glycerol, 1 mM DTT). MBP-TREX1$_{1–242}$ was eluted with the equilibrium buffer containing 10 mM L-maltose. The fractions were analyzed by 10% SDS-PAGE and pure MBP-TREX1$_{1–242}$ fractions were combined, mixed with PreScission protease (20 units, APEXBIO, Cat. #: K1101), and incubated at 4°C overnight without shaking. Following MBP-tag cleavage, the sample was spun down at 4°C to remove the precipitate. The supernatant was bound to a Heparin column (1 ml). The column was washed extensively with a low salt buffer (50 mM Tris–HCl, pH 7.5, 100 mM NaCl, 10% glycerol, 1 mM DTT), and the protein was then eluted out with the same buffer with a salt gradient (100–1000 mM NaCl). The fractions were analyzed by 10% SDS-PAGE. Pure TREX1$_{1–242}$ fractions were combined and concentrated with a 10 kDa cut-off Amicon filter at 4°C. The protein concentration was determined by the Bradford assay. The protein (2.4 mg) was aliquoted, flash frozen with liquid N$_2$, and stored at -80°C. TREX1$_{1–242}$-D18N was overexpressed and purified following the same procedures described above.

The plasmid (pET28a-hPARP1) that expresses the N-terminal his-tagged human PARP1 was obtained from Professor Ilya Finkelstein (University of Texas at Austin), which was originally constructed by Professor John Pascal (Université de Montréal). The protein was overexpressed and purified following a published protocol (58).

Enzymatic removal of 3′-PUA–OxyLys–peptides

Typical reactions (5–10 μl) containing 1× buffer (TDP1: 50 mM Tris–HCl, pH 7.5, 50 mM NaCl, 5 mM MgCl$_2$; APE1: 20 mM Tris-acetate, pH 7.9, 50 mM potassium acetate, 10 mM magnesium acetate, 1 mM DTT; TREX1, Polε, Polδ, and WRN: 20 mM Tris–HCl, pH 7.5, 5 mM MgCl$_2$, 2 mM DTT, 0.1 mg/ml BSA; MRN: 25 mM Tris–HCl, pH 7.5, 60 mM NaCl, 2 mM MnCl$_2$, 1 mM DTT), and indicated concentrations of substrates and enzymes were incubated at 37°C for 10–60 min. The reactions with TDP1, APE1, Polε, Polδ, MRN or WRN were quenched by an equal volume of loading buffer (85% formamide, 80 mM EDTA, 0.2% SDS, 200 pmol oligo O3). The reactions with TREX1 were quenched by three volumes of cold ethanol, dried in a speed vacuum and resuspended in a loading buffer (85% formamide, 80 mM EDTA, 200 pmol oligo O3). All samples were heated at 90°C for 5 min and quickly put on ice, followed by analysis with a 20% urea–PAGE gel (40 × 32 × 0.04 cm). The gel was run at room temperature at 75 W for 20 min and then with a constant power (60 W) until the bromophenol blue migrated to the middle (for TREX1, Polε, Polδ, MRN and WRN) or a quarter of the gel from the bottom (for TDP1 and APE1).

Steady-state kinetic study of 3′-PUA–OxyLys–peptide$_{10mer}$ removal within nicked DNA

Typical reactions (5 μl) with nicked DNA (0.04–2 μM for TDP1, 0.02–4 μM for APE1) bearing 3′-PUA–OxyLys–peptide$_{10mer}$ and 5′-phosphate, 1x buffer (TDP1: 50 mM Tris–HCl, pH 7.5, 50 mM NaCl, 5 mM MgCl$_2$; APE1: 20 mM Tris-acetate, pH 7.9, 50 mM potassium acetate, 10 mM magnesium acetate, 1 mM DTT), and enzymes (10 nM TDP1, 5 nM APE1) were incubated at 37°C for 5–10 min. The reactions were quenched by an equal volume of loading buffer (85% formamide, 80 mM EDTA, 0.2% SDS, 200 pmol oligo O3) and frozen on dry ice. The samples were heated at 90°C for 5 min and quickly put on ice, followed by analysis with 20% urea–PAGE. The gel (20 × 16 × 0.08 cm) was run at room temperature at 25 W for 20 min and then with a constant power (18 W) until the bromophenol blue migrated to a quarter of the gel from the bottom. The reaction rates were plotted against the concentration of the substrates using the Menten-Michaelis equation ($v = V_{max}$ [S]/(K_m +[S])) by Prism 6.0. The k_{cat} was calculated using the equation $k_{cat} = V_{max}/[E]$.

Preparation and enzymatic removal of reduced 3′-PUA–histone DPCs

A reaction mixture (2 ml) including an AP site-containing single-strand oligo (Table 1, O5, 1 nmol) and histone H2B or H4 (10 nmol) in a HEPES buffer (10 mM, pH 7.5) was

incubated at 37°C for 19 h, followed by addition of freshly prepared $NaBH_3CN$ (final concentration = 100 mM) and SDS (final percentage = 0.1%) and incubating at 37°C for 6 h. After that, the sample was dried overnight in a speed vacuum. The residue was resuspended in 100 μl H_2O followed by ethanol precipitation. The sample was then resuspended in a loading buffer (25 mM HEPES, pH 7.5, 40% glycerol, 0.2% SDS), heated at 90°C for 10 min, and analyzed by a 15% SDS-PAGE gel (20 × 16 × 0.8 cm). The gel was run at room temperature with a constant power (15 W) until the bromophenol blue dye migrated to the bottom of the gel. The DPC band was cut, smashed, and soaked in an eluting buffer (3 ml, 0.2 M NaCl, 1 mM EDTA, 0.1% SDS). After rotating the tube at room temperature overnight, the sample was spun down. The supernatant was then carefully taken out, concentrated, and exchanged extensively (12–16 times, 10-fold dilution/time) to a HEPES buffer (50 mM, pH 7.5) using a 3.0 kDa cut-off Amicon centrifugal filter at 16°C. The DPC concentration was determined by 15% SDS-PAGE using oligo O5 as a reference. The DPC sample (40–60 pmol) was aliquoted and stored at –80°C.

The above isolated 3′-PUA–histone DPC (5 pmol) was mixed with a complementary strand (Table 1, O7 or O8, 6 pmol) in a sodium phosphate buffer (10 mM, pH 7.0) containing 100 mM NaCl. The mixture was heated at 90°C for 1 min, followed by cooling down to room temperature. Typical reactions (5 μl) containing hybridized 3′-PUA–histone DPC (300 fmol, final concentration = 60 nM), 1× buffer (TDP1: 50 mM Tris–HCl, pH 7.5, 50 mM NaCl, 5 mM $MgCl_2$; APE1: 20 mM Tris-acetate, pH 7.9, 50 mM potassium acetate, 10 mM magnesium acetate, 1 mM DTT; TREX1: 20 mM Tris–HCl, pH 7.5, 5 mM $MgCl_2$, 1 mM DTT, 0.1 mg/ml BSA), and indicated concentrations of enzyme were incubated at 37°C for 60 min. All reactions were quenched by an equal volume of loading buffer (50 mM HEPES, pH 7.5, 40% glycerol, 0.2% SDS) and analyzed by a 15% SDS-PAGE gel (20 × 16 × 0.08 cm). The gel was run at room temperature with a constant power (5 W) until the bromophenol blue migrated to the middle.

Preparation and nuclease treatment of 3′-PUA–PARP1 DPC

To prepare the 3′-PUA–PARP1 DPC under native conditions, a typical reaction (50 μl) containing an AP site within 42-nt double-stranded DNA (20 pmol, hybridized O7 and O29 or O8 and O30) and PARP1 (50 pmol) in a reaction buffer (25 mM sodium phosphate, pH 7.0, 25 mM NaCl) was incubated at 37°C for 4 h. The reaction sample was briefly centrifuged and the supernatant was carefully taken out. To investigate the 3′-PUA–PARP1 DPC repair by TREX1, a typical reaction (5 μl) containing the above reaction mixture (final concentration of total DNA and DPC = 60 nM), 1× buffer (20 mM Tris–HCl, pH 7.5, 5 mM $MgCl_2$, 2 mM DTT, 0.1 mg/ml BSA), and an indicated concentration of $TREX1_{1–242}$ was incubated at 37°C for 60 min. The reaction was quenched by an equal volume of loading buffer (50 mM HEPES, pH 7.5, 40% glycerol, 0.2% SDS, 2 mM DTT), and analyzed by an 8% SDS-PAGE gel (20 × 16 × 0.08 cm). The gel was run at room temper-

ature with a constant power (5 W) until the bromophenol blue migrated to the middle.

To prepare the denatured 3′-PUA–PARP1 DPC, a typical reaction (2 ml) containing an AP site within 42-nt double-stranded DNA (400 pmol, hybridized O7 and O29 or O8 and O30) and PARP1 (1 nmol) in a reaction buffer (25 mM sodium phosphate, pH 7.0, 25 mM NaCl) was incubated at 37°C for 4 h. The reaction was quenched by adding SDS to a final percentage of 0.1% and freshly prepared $NaBH_4$ to a final concentration of 0.1 M, followed by incubating at 4°C for 1 h. The quenched mixture was then concentrated to ~200 μl with a 3.0 kDa cut-off Amicon centrifugal filter, followed by ethanol precipitation. The residue was resuspended in a loading buffer (70 μl, 50 mM HEPES, pH 7.5, 40% glycerol, 0.2% SDS, 1 mM DTT) and analyzed by an 8% SDS-PAGE gel (12 × 8 × 0.15 cm). The gel was run at 4°C with a constant power (3 W) until the bromophenol blue dye migrated to 1/3 of the gel from the top. The DPC band was cut, smashed, and soaked in an eluting buffer (1.4 ml, 0.2 M NaCl, 1 mM EDTA, 0.1% SDS,1 mM DTT). After rotating the tube at 4°C overnight, the sample was spun down. The supernatant was then carefully taken out, concentrated, and exchanged extensively (16 times, 10-fold dilution/time) to a HEPES buffer (50 mM, pH 7.5, 100 mM NaCl, 1 mM DTT) using a 10 kDa cut-off Amicon centrifugal filter at 4°C. The DPC concentration was determined by 8% SDS-PAGE using oligo O29 or O30 as a reference. The DPC sample (~11 pmol) was aliquoted and stored at –80°C. To investigate the nuclease repair of denatured 3′-PUA–PARP1 DPC, a typical reaction (10 μl) containing the isolated 3′-PUA–PARP1 DPC (600 fmol, final concentration = 60 nM), 1x buffer (TDP1: 50 mM Tris–HCl, pH 7.5, 50 mM NaCl, 5 mM $MgCl_2$, 1 mM DTT; APE1: 20 mM Tris-acetate, pH 7.9, 50 mM potassium acetate, 10 mM magnesium acetate, 1 mM DTT; $TREX1_{1–242}$: 20 mM Tris–HCl, pH 7.5, 5 mM $MgCl_2$, 1 mM DTT, 0.1 mg/ml BSA), and an indicated concentration of TDP1, APE1 or $TREX1_{1–242}$ was incubated at 37°C for 60 min. The reaction was quenched by an equal volume of loading buffer (50 mM HEPES, pH 7.5, 40% glycerol, 0.2% SDS, 1 mM DTT) and analyzed by an 8% SDS-PAGE gel (12 × 8 × 0.15 cm). The gel was run at 4°C with a constant power (3 W) until the bromophenol blue migrated to the middle.

Preparation and enzymatic removal of 3′-PUA–PARP1 peptide cross-links

A typical reaction (1.5 ml) containing an AP site within 42-nt double-stranded DNA (300 pmol, hybridized O7 and O30 or O8 and O30) and PARP1 (750 pmol) in a reaction buffer (25 mM sodium phosphate, pH 7.0, 25 mM NaCl) was incubated at 37°C for 4 h. The reaction sample was then mixed with proteinase K (8 units), incubated at room temperature for 1.5 h, and then concentrated to ~100 μl with a 3.0 kDa cut-off Amicon centrifugal filter. The concentrated sample was mixed with a sodium phosphate buffer (100 μl, 10 mM, pH 7.0) and treated by $NaBH_4$ (0.1 M, 4°C, 1 h) to stabilize the unreacted AP sites. The mixture was then subjected to phenol-extraction (two times) and ethanol precipitation (two times). The residue was resuspended with a

sodium phosphate buffer (100 μl, 10 mM, pH 7.0). The concentration of total 3′-PUA-peptide adducts was measured by urea–PAGE using the 3′-PUA–OxyLys–peptides as references. To investigate whether 3′-PUA-peptide adducts can be removed by TDP1, APE1 and TREX1, typical reactions (20 μl) containing 3′-PUA-peptide adducts (2 pmol, final concentration = 100 nM), 1× buffer (TDP1: 50 mM Tris–HCl, pH 7.5, 50 mM NaCl, 5 mM MgCl$_2$; APE1: 50 mM potassium acetate, pH 7.9, 20 mM Tris-acetate, 10 mM magnesium acetate, 1 mM DTT; TREX1: 20 mM Tris–HCl, pH 7.5, 5 mM MgCl$_2$, 2 mM DTT, 0.1 mg/ml BSA), and indicated concentrations of enzymes were incubated at 37°C for 60 min. Aliquots (5 μl) of the reactions were quenched by an equal volume of loading buffer (85% formamide, 80 mM EDTA, 0.2% SDS, 200 pmol oligo O3). The samples were heated at 90°C for 3 min and quickly put on ice, followed by analysis with a 20% urea–PAGE gel (40 × 32 × 0.04 cm). The gel was run at room temperature at 75 W for 20 min and then with a constant power (60 W) until the bromophenol blue migrated to the bottom (for TDP1 and APE1) or half of the gel (for TREX1).

RESULTS AND DISCUSSION

### Schiff base 3′-PUA–histone DPCs are unstable but long-lived

Several studies have demonstrated that the hydrolysis of Schiff base 3′-PUA–protein DPCs can be slow, but none of their half-lives has been reported (17,25,29,30,50). Here, we measured the half-lives of 3′-PUA–histone DPCs under physiological temperature and pH. Specifically, an AP site-containing oligo (Table 1, O5) was prepared by treating 2′-deoxyuracil (dU) with *Escherichia coli* uracil–DNA glycosylase, followed by reacting with histone H2B or H4. To determine the DPC identity (Scheme 2, Schiff base AP-histone or 3′-PUA–histone DPC), the reaction products were stabilized by NaBH$_3$CN and resolved by SDS-PAGE (Supplementary Figure S1A). The DPCs were isolated, digested by proteinase K, and analyzed by urea–PAGE (Supplementary Figure S1B). All proteolyzed products migrated faster than the AP site and slightly slower than the NaOH-incised AP site, suggesting that the DPCs are exclusively 3′-PUA–histone DPCs (Supplementary Figure S1C). To determine their half-lives, after reacting the AP site to histones, 3′-PUA–histone DPCs were directly isolated by SDS-PAGE without NaBH$_3$CN stabilization and exchanged to a HEPES buffer (10 mM, pH 7.5) at 4°C. A portion of the DPCs decomposed at this step (Supplementary Figure S2A) likely due to the high concentration (~375 mM) of Tris in the SDS-PAGE gels that mediated the transimination. Following incubating at 37°C for a period of time (0–56 h), the remaining 3′-PUA–histone DPCs were analyzed by SDS-PAGE (Supplementary Figure S2B, C). The half-lives of 3′-PUA-H2B and 3′-PUA-H4 DPCs are 10 ± 0.4 and 14 ± 0.1 h, respectively, which are more stable than Schiff base 5-formylcytosine-histone ($t_{1/2}$ = ~1.8 h (59)) and 5-formyluracil-histone ($t_{1/2}$ = ~28 min (60)) DPCs. Considering that the average length of the human cell cycle is ~24 h, the long-lived Schiff base 3′-PUA–protein DPCs must be promptly eradicated because 3′-OH is required for DNA synthesis and strand ligation.

Synthesis of 3′-PUA-OxyLys by oxime ligation

The major goal of this study is to identify the enzyme(s) that repairs 3′-PUA–protein DPCs. Previous studies have demonstrated that 3′-PUA-hOGG1 DPC cannot be removed by APE1 (50). Both APE1 and TDP1 failed to remove 3′-PUA–PARP1 DPC (28,53). Emerging evidence indicates that proteolysis is required for efficient DPC removal (24,61–67). Indeed, 3′-PUA–PARP1 DPC has been demonstrated to be degraded by the proteasome and Spartan in mammalian cells (53,54). Therefore, we asked whether 3′-PUA-peptide cross-links produced from DPC proteolysis can be enzymatically removed. Although protease (e.g. proteinase K)-digested DPCs can be used as substrates to search for the potential repair enzymes, the inefficient DPC preparation and heterogenous proteolyzed products make them not suitable for kinetic studies. In addition, although Schiff base 3′-PUA–protein DPC is long-lived at physiological temperature (37°C), it is extremely unstable under heating at a higher temperature (e.g. 90°C), which is often required to separate the DNA strands before urea–PAGE analysis. To overcome these limitations, we developed a chemical approach to synthesize a stable adduct (3′-PUA-OxyLys) that closely resembles the proteolysis product of 3′-PUA–protein DPCs by reacting a 3′-PUA-containing oligonucleotide and an aminooxylysine (OxyLys) through oxime ligation (Scheme 3). Compared to 3′-PUA–histone DPCs, the linkage in 3′-PUA-OxyLys has only one difference that the ε-carbon is replaced by an oxygen atom. Our rationale is that if the repair enzyme(s) fails to remove 3′-PUA-OxyLys, it less likely can repair the larger DNA–peptide/protein adducts.

We first screened the reported enzymatic and chemical approaches to prepare 3′-PUA. Treating the AP site by endonuclease III has been suggested to generate 3′-PUA, however, several studies have demonstrated that this enzymatic reaction also yields hydrolyzed 3′-PUA (3′-deoxyribose phosphate; 3′-dRP, Scheme 1) that will also react with OxyLys (68,69). We tested several other chemical conditions that have been suggested to produce 3′-PUA from an AP site (11,69–71). Specifically, an AP site-containing oligo (Table 1, O4 or O5) was reacted with NaOH or *N,N*′-dimethylethylenediamine, or heated. The reaction products were characterized by urea–PAGE and/or MALDI-TOF mass spectrometry. NaOH treatment yielded similar amounts of β and δ-elimination products, and the predominant β-elimination product is 3′-dRP (Supplementary Figure S3). Reacting the AP site with *N,N*′-dimethylethylenediamine mainly yielded the β-elimination product, but the hydrolysis of the iminium linkage is slow, resulting in a low yield of 3′-PUA (Supplementary Figure S4). Heating (10 mM sodium phosphate, pH 7.0, 95°C, 15–120 min) exclusively generated the β-elimination product and ~95% of that is 3′-PUA within the first 30 min (Supplementary Figure S5). Longer heating (e.g. 60 min) increased the yield of 3′-PUA but it also produced more 3′-dRP (Supplementary Figures S5B and S6). Therefore, in the following work, heating the AP site (10 mM sodium phosphate, pH 7.0) at 95°C for 30 min was performed to prepare 3′-PUA.

Next, *tert*-butyloxycarbonyl (Boc) protected OxyLys was synthesized as previously described (55,56), followed by re-
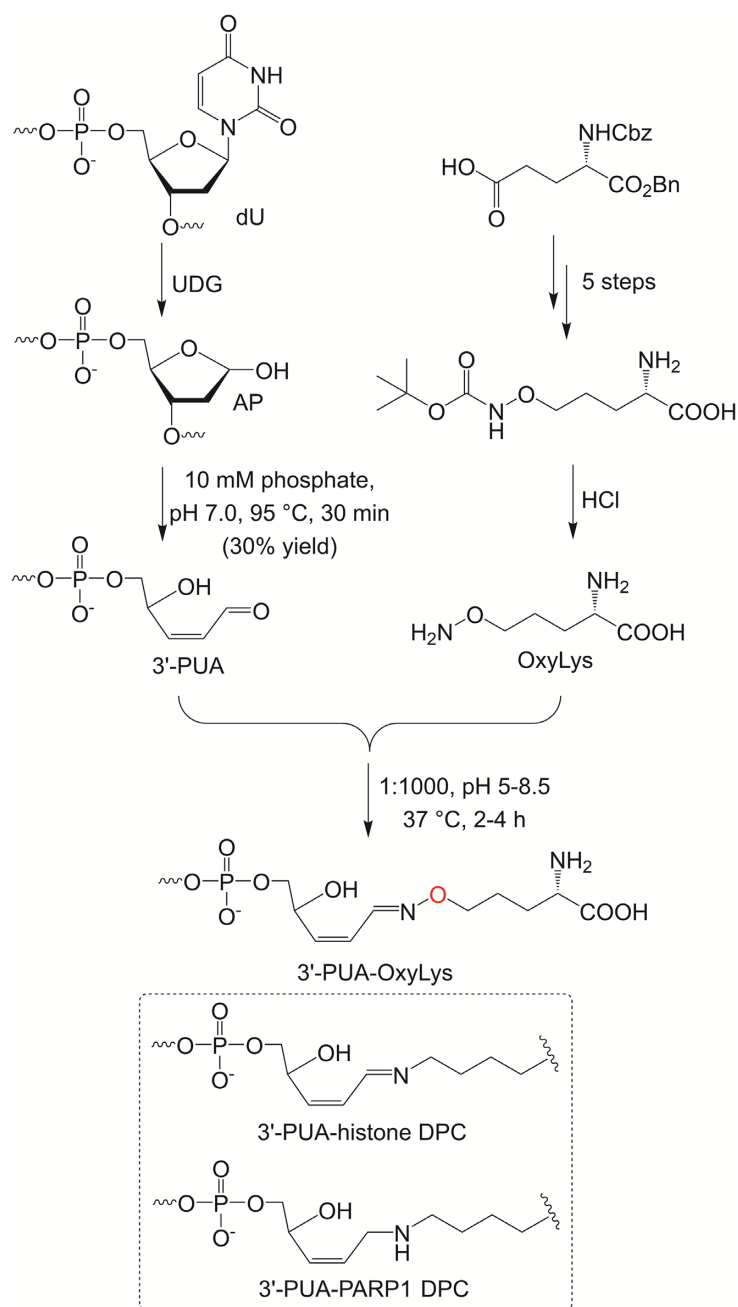
Scheme 3. Synthesis of 3′-PUA-OxyLys by oxime ligation.

moving the Boc group by HCl to yield OxyLys (Scheme 3, Supplementary Figures S7 and S8). Urea-PAGE analysis indicated complete conjugation of 3′-PUA to OxyLys at all tested conditions (Supplementary Figure S9A). The desired adduct was purified by urea–PAGE. MALDI-TOF mass spectrometry characterization confirmed the imine formation instead of a Michael addition reaction by the molecular weight difference of a water molecule that was lost after the conjugation (Supplementary Figure S9B). The adduct was stable after heating (70°C for 1 h, or 95°C for 10 min) or NaOH treatment (0.1 M, 37°C, 1 h, Supplementary Figure S9C), suggesting that the cross-linking occurred exclusively through oxime ligation since the adduct will decom-

pose under these conditions if the adduct was formed from the amine (48). This approach allows us to synthesize a nanomole scale of 3′-PUA-OxyLys (Table 1, P1) that is sufficient for most, if not all, biochemical experiments. Site-specific 3′-PUA–OxyLys–peptide adducts (Table 1, P2–4) can be prepared similarly (see below).

TDP1 removes 3′-PUA-OxyLys within nicked DNA

With 3′-PUA-OxyLys in hands, we first asked whether it can be enzymatically removed within the nicked DNA bearing a 3′-PUA-OxyLys and 5′-phosphate (Figure 1A) that structurally mimics the 3′-PUA–protein DPCs (Scheme 2).
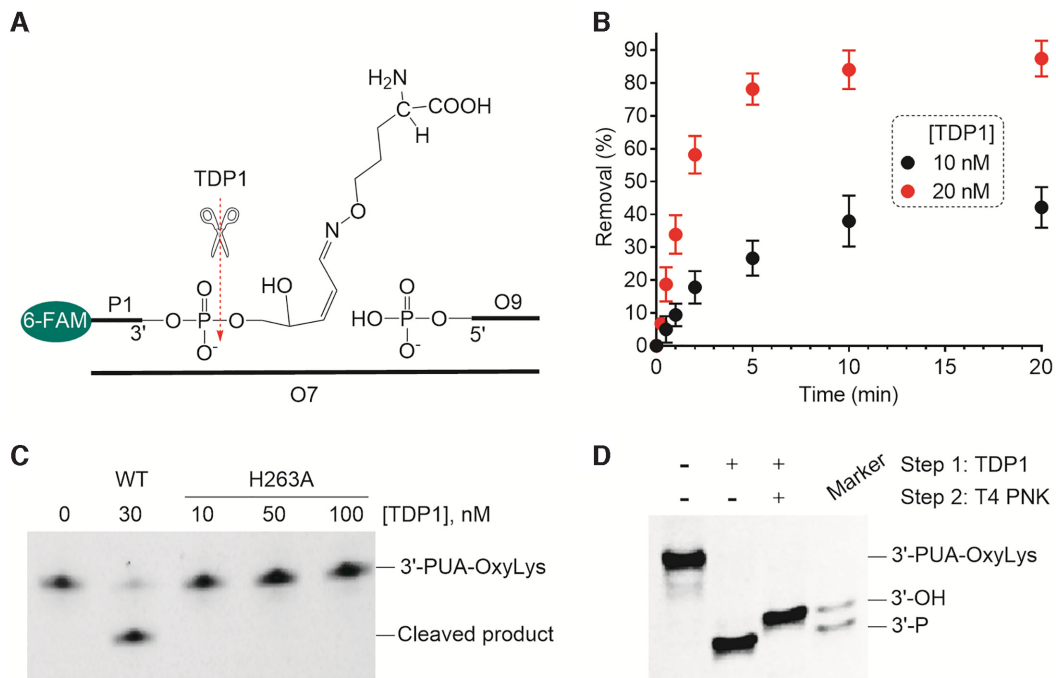
Figure 1. Removal of 3′-PUA-OxyLys within nicked DNA by TDP1. (**A**) The structure of nicked DNA containing 3′-PUA-OxyLys and 5′-phosphate. The red dashed arrow illustrates the excision site of TDP1. (**B**) A plot showing the efficiency of TDP1 (10 or 20 nM) to remove 3′-PUA-OxyLys within nicked DNA (50 nM) at 37 °C as a function of time. The data is from three independent experiments. (**C**) A representative 20% urea–PAGE gel showing the removal of 3′-PUA-OxyLys within the nicked DNA (80 nM) by wild type (WT) but not the catalytically inactive (H263A) TDP1. The reactions were carried out at 37°C for 30 min. (**D**) A representative 20% urea–PAGE gel showing the removal of 3′-PUA-OxyLys within the nicked DNA by TDP1 with or without an additional treatment by T4 polynucleotide kinase (T4 PNK). Step 1, 3′-PUA-OxyLys (80 nM) was treated by TDP1 (50 nM) at 37°C for 30 min. Step 2, to the mixture in Step 1, T4-PNK (0.5 unit/μl) was added and incubated at 37°C for 30 min. The urea–PAGE gels in (C) and (D) were scanned using the fluorescence of 6-FAM.

This structure represents the conditions in which the 3′-PUA–protein DPC is generated from a single isolated AP site and the DPC repair is replication-independent. To address this question, a 25-nt oligo was first enzymatically phosphorylated at the 5′-terminus (Table 1, O9). The complete 5′-phosphorylation was confirmed by MALDI-TOF mass spectrometry (Supplementary Figure S10A). Next, the 5′-phosphorylated oligo and 3′-PUA-OxyLys were hybridized to the complementary strand (Table 1, O7). The nicked DNA was purified and further verified by native PAGE (Supplementary Figure S10B). Human TDP1 was first tested due to its ability of removing 3′-phosphotyrosine and other 3′-end blocks (72,73). Both wild type (WT) and catalytically inactive mutant (H263A) TDP1 were purified from *E. coli* cells (Supplementary Figure S11A). We found that WT, but not H263A TDP1, removed 3′-PUA-OxyLys (Figure 1B-C, Supplementary Figure S11B). Such reaction yielded a product that migrated the same with the oligo marker bearing a 3′-phosphate (Figure 1D). An additional treatment with T4 polynucleotide kinase (T4 PNK) that has 3′-phosphatase activity yielded a product that migrated the same with the marker containing a 3′-OH. Based on these observations, we conclude that TDP1 removed 3′-PUA-OxyLys and yielded a 3′-phosphate group. This finding agrees with the previous observation by Wilson *et al.* that TDP1 repaired a model substrate (C7-NH$_2$, Scheme 1) that mimics the proteolyzed 3′-PUA–PARP1 DPC (53).

APE1 removes 3′-PUA-OxyLys within nicked DNA

Next, we tested human APE1, a multifunctional enzyme that has endonuclease activity to incise 5′-side of the AP site, and 3′ to 5′ exonuclease activity to remove 3′-PUA and 3′-mismatched nucleotides (74). Different from the previous result that APE1 failed to repair the model substrate, C7-NH$_2$ (53), APE1 efficiently removed 3′-PUA-OxyLys within the nicked DNA (Figure 2A-B, Supplementary Figure S12), and the major product migrated the same as the oligo marker bearing a 3′-OH (Figure 2C). A small amount of 1-nt shorter exonuclease product was also observed. Thus, we conclude that APE1 is able to remove 3′-PUA-OxyLys within nicked DNA and generate a 3′-OH. This is further supported by the observation that 3′-PUA-OxyLys was efficiently removed by exonuclease III (Supplementary Figure S13), the *E. coli* APE1 homolog. The finding that APE1 removes 3′-PUA-OxyLys is surprising as APE1 utilizes the same active site for both endonuclease and exonuclease activity, however, conjugating a small methoxyamine (75,76) or OxyLys (data not shown) to an AP site completely blocks the AP-endonuclease activity. Such difference could be explained by the distinct mechanisms revealed by the structural studies. APE1 incises the endo-AP site via flipping the lesion out of the DNA helical cavity and into its active site (77,78). Therefore, modifications of the AP site could inhibit the binding to APE1. Whereas APE1's exonuclease activity involves placing the 3′-group within the
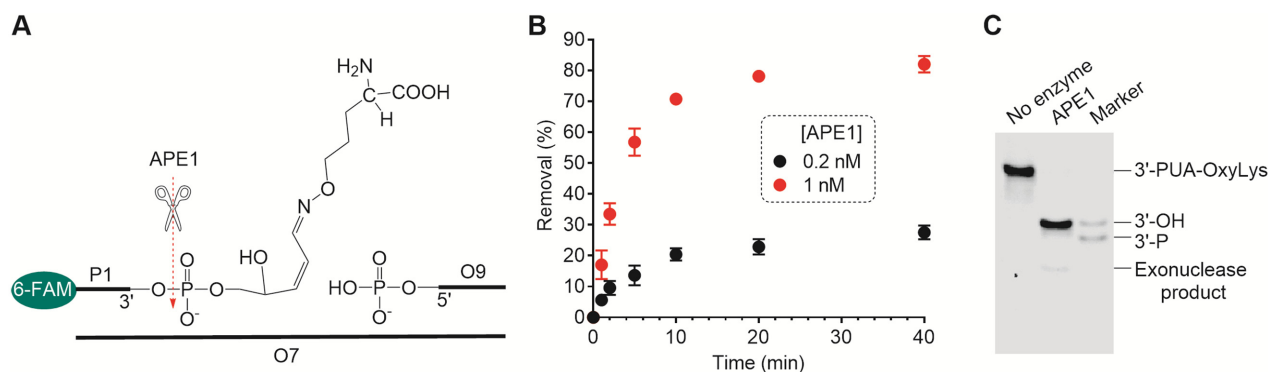
Figure 2. Removal of 3′-PUA-OxyLys within nicked DNA by APE1. (**A**) The structure of nicked DNA containing 3′-PUA-OxyLys and 5′-phosphate. The red dashed arrow illustrates the excision site of APE1. (**B**) A plot showing the removal of 3′-PUA-OxyLys within nicked DNA (50 nM) by APE1 (0.2 or 1 nM) at 37°C as a function of time. The data is from three independent experiments. (**C**) A representative 20% urea–PAGE gel showing the removal of 3′-PUA-OxyLys within the nicked DNA (80 nM) by APE1 (20 nM) at 37°C for 30 min. The gel was scanned using the fluorescence of 6-FAM.

intra-helical DNA cavity by a non-base flipping mechanism ([79]), suggesting that APE1 could accommodate and process bulky 3′-PUA-OxyLys, and even larger 3′-obstructive DNA lesions, including 3′-PUA–OxyLys–peptides and 3′-PUA–histone DPCs (see below).

TREX1 removes 3′-PUA-OxyLys within nicked DNA

We accidentally discovered that TREX1 is able to remove 3′-PUA-OxyLys. TREX1 is an effective and non-processive human 3′ to 5′ exonuclease that depletes the cytosolic DNA to prevent the autoimmune response ([80]). *TREX1* mutations cause several human autoimmune diseases, such as Aicardi-Goutieres syndrome and familial chilblain lupus ([81,82]). TREX1 has a long N-terminal catalytic domain (1–242) that maintains the full exonuclease activity and a short C-terminal transmembrane domain (243–314) that anchors to the endoplasmic reticulum ([83]). In response to the genotoxic stress, TREX1's expression is upregulated and a portion of the protein translocates from cytoplasm to the nucleus ([84,85]), but its function in the latter is not clear. It has been suggested that TREX1 is not directly involved in DNA repair as it is unable to remove several 3′-obstructive DNA lesions including 3′-phosphate, 3′-phosphoglycolate, and 3′-phosphotyrosine ([86,87]). Agreeing with the previous result, 3′-phosphate prevented the processing of native single-strand oligo by $TREX1_{1-242}$ (Supplementary Figure S14). Strikingly, $TREX1_{1-242}$ efficiently removed the 3′-PUA-OxyLys within single-strand DNA and further degraded the DNA strand (Supplementary Figure S14). To determine whether 3′-PUA-OxyLys within the nicked DNA is a substrate of TREX1, all free 3′-OH termini of the nicked DNA substrate were blocked by phosphorylation (Figure 3A) to prevent the undesired DNA degradation. We found that $TREX1_{1-242}$ removed the 3′-PUA-OxyLys in both enzyme concentration-dependent (Figure 3B) and time-dependent manners (Figure 3C, Supplementary Figure S15B). This is ascribed to TREX1's exonuclease activity as the catalytically inactive mutant (D18N) failed to remove 3′-PUA-OxyLys (Figure 3D). To our knowledge, this is the first time to reveal that TREX1 can remove a bulky 3′-obstructive lesion *in vitro*.

TDP1, APE1, and TREX1 remove 3′-PUA–OxyLys–peptides within nicked DNA

Having identified that TDP1, APE1, and TREX1 can repair 3′-PUA-OxyLys within nicked DNA, we then asked whether these nucleases can remove longer peptide adducts which will more likely be produced following the DPC proteolysis repair. To address this question, we synthesized two OxyLys-containing peptides by solid-phase peptide synthesis ([56]). The 5-mer peptide is derived from human histone $H4_{13-17}$ (NH_2-GGAK$_{16}$R-COOH) with the substitution of Lys16 with OxyLys. The 10-mer one is from $H4_{1-10}$ (NH_2-SGRGK$_5$GGKGL-COOH) with the replacement of Lys5 by OxyLys. The 3′-PUA–OxyLys–peptide$_{5mer}$ and 3′-PUA–OxyLys–peptide$_{10mer}$ adducts (Table 1, P2–3) were synthesized, purified, and characterized similarly to 3′-PUA-OxyLys (Supplementary Figures S16 and S17). The corresponding nicked substrates (Figure 4A) containing 3′-PUA–OxyLys–peptide and 5′-phosphate were purified and further verified by native PAGE (Supplementary Figure S18). As shown in Figure 4B, TDP1 removed the 5-mer adduct 1.3-fold more efficiently than the 1-mer one, and removed the 10-mer adduct similarly to the 1-mer cross-link. When the peptide length increases from 1 to 5 and 10-mer, the adduct removal efficiency of APE1 decreased by 26% and 48%, respectively (Figure 4C). TREX1 removed the 5-mer adduct similarly to the 1-mer one but the efficiency decreased by 47% when the adduct increases to 10-mer (Figure 4D). Taken together, these results suggested that TDP1, APE1 and TREX1 can remove 3′-PUA–OxyLys–peptide cross-links within nicked DNA. Among all three nucleases, TDP1 accommodates the longer peptide adduct better than APE1 and TREX1, and a larger adduct generally inhibits the repair by the latter two.

The steady-state kinetic constants of adduct removal by TDP1 and APE1 were determined using the nicked DNA containing a 3′-PUA–OxyLys–peptide$_{10mer}$ and a 5′-phosphate. The Michaelis-Menten saturation curves were shown in Supplementary Figure S19 and the kinetic constants were summarized in Table 2. TDP1 removed 3′-PUA–OxyLys–peptide$_{10mer}$ with the catalytic efficiency (k_{cat}/K_m) of 2.48 ± 0.44 μM^{-1}min^{-1}, which is ~10-times lower than removing 3′-phosphotyrosine within the nicked DNA
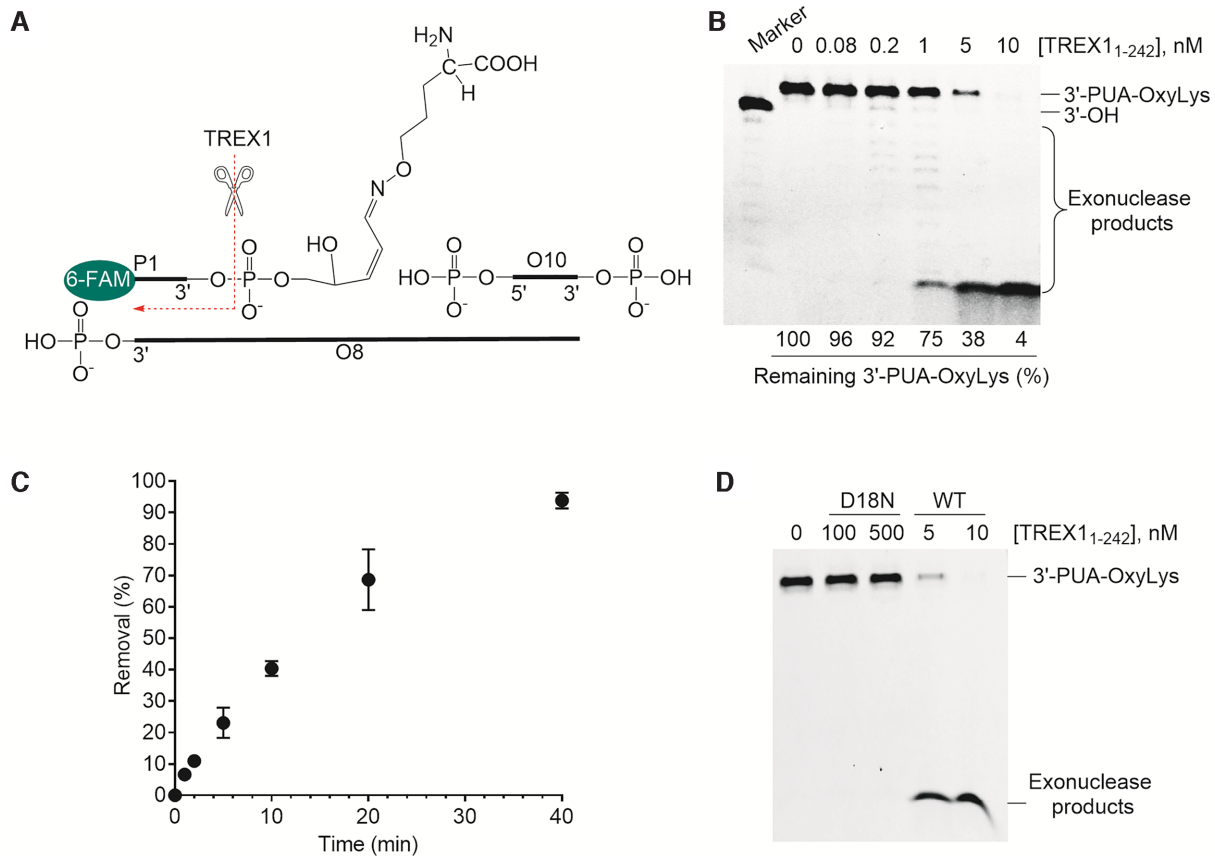
Figure 3. Removal of 3′-PUA-OxyLys within nicked DNA by TREX1. (**A**) The structure of nicked DNA containing 3′-PUA-OxyLys and 5′-phosphate. The free 3′-termini were blocked by phosphorylation to prevent the undesired degradation by TREX1. The red dashed arrow illustrates the processing of 3′-PUA-OxyLys by TREX1. (**B**) A representative 20% urea–PAGE gel showing the removal of 3′-PUA-OxyLys within nicked DNA (20 nM) by indicated concentrations of TREX1$_{1-242}$ at 37°C for 30 min. (**C**) A plot showing the removal efficiency of 3′-PUA-OxyLys within nicked DNA (50 nM) by TREX1 (5 nM) at 37°C as a function of time. The data is from three independent experiments. (**D**) A representative 20% urea–PAGE gel showing the removal of 3′-PUA-OxyLys within the nicked DNA by increasing concentrations of wild type (WT) or catalytically inactive (D18N) TREX1$_{1-242}$. The reactions were carried out by incubating the substrate (20 nM) and indicated concentration of enzyme at 37°C for 30 min. The urea–PAGE gels in (**B**) and (**D**) were scanned using the fluorescence of 6-FAM.

($k_{cat}/K_m = \sim25$ μM^{-1}min^{-1}) (88). Removal of 3′-PUA–OxyLys–peptide$_{10mer}$ by APE1 ($k_{cat}/K_m = 4.38 \pm 0.68$ μM^{-1}min^{-1}) is 1.8-fold higher than TDP1. It's difficult (if possible) to determine the kinetic constants of TREX1 specifically for 3′-PUA–OxyLys–peptide$_{10mer}$ removal as it will further bind to the product and effectively degrade the polynucleotides. Therefore, we compared the relative efficiency of TREX1 and APE1 by determining the total 3′-PUA–OxyLys–peptide$_{10mer}$ removal within nicked DNA as a function of time under the same enzyme concentration. Under a single-turnover condition (20 nM substrate, 40 nM enzyme), TREX1 is slightly more efficient than APE1 (Supplementary Figure S20A). An opposite result was observed under a multiple-turnover condition (50 nM substrate, 5 nM enzyme) but the difference is small (∼1.5-fold, Supplementary Figure S20B). Thus, we conclude that TREX1 has a comparable rate to APE1 for removing 3′-PUA–OxyLys–peptide$_{10mer}$ within nicked DNA.

The finding that TREX1 effectively excises 3′-PUA–OxyLys–peptide adducts encourages us to ask whether other human 3′ to 5′ exonucleases have similar activity. To address this question, we compared side-by-side the activity of TREX1 and another four prominent human 3′ to

5′ exonucleases including DNA polymerase epsilon (Polε), polymerase delta (Polδ), Mre11–Rad50–Nbs1 (MRN), and Werner syndrome protein (WRN), which play important roles in DNA replication and/or repair (89). As shown in Supplementary Figure S21, among all four enzymes, only Polε is able to remove the 3′-PUA–OxyLys–peptide$_{10mer}$ adduct in an enzyme concentration-dependent manner. However, compared to TREX1, the activity of Polε is negligible. Specifically, following incubating the 3′-PUA–OxyLys–peptide cross-link (40 nM) with TREX1 or Polε (20 nM) at 37 °C for 30 min, nearly 90% of the adduct was removed by TREX1, while only ∼2% of the adduct was excised by Polε (Supplementary Figure S21B). These results suggest that the 3′ to 5′ exonuclease activity of TREX1, but not Polε, Polδ, MRN, or WRN, likely contributes to the direct repair of 3′-PUA-peptide cross-links.

Effect of flanking DNA structure on 3′-PUA–OxyLys–peptide$_{10mer}$ removal

3′-PUA–protein DPCs could locate within different flanking DNA structure other than a nick. For example, clustered lesions in which two or more lesions, such as AP
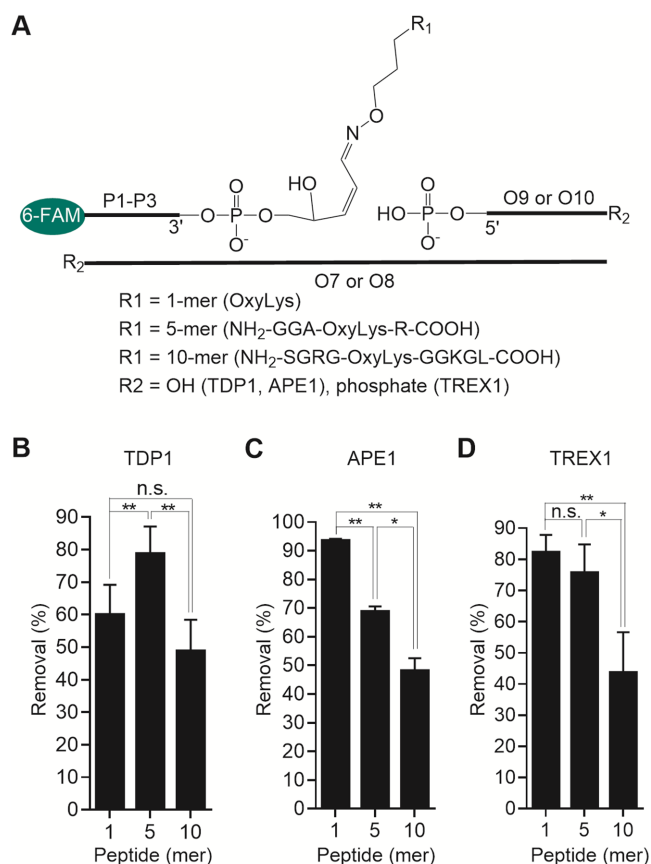
A

R1 = 1-mer (OxyLys)
R1 = 5-mer (NH$_2$-GGA-OxyLys-R-COOH)
R1 = 10-mer (NH$_2$-SGRG-OxyLys-GGKGL-COOH)
R2 = OH (TDP1, APE1), phosphate (TREX1)

B TDP1 **C** APE1 **D** TREX1

Figure 4. Removal of 3′-PUA–OxyLys–peptide cross-links within nicked DNA by TDP1, APE1 and TREX1. (**A**) Illustration of nicked DNA containing 3′-PUA–OxyLys–peptides and 5′-phosphate. (**B–D**) The plots showing the efficiency of adduct removal as a function of cross-linked peptide length by TDP1 (B), APE1 (C), and TREX1 (D). In (B) and (C), the reactions were carried out by incubating the substrate (80 nM) with TDP1 (30 nM) or APE1 (10 nM) at 37°C for 30 min. In (D), the reactions were performed by incubating the substrate (20 nM) with TREX1 (10 nM) at 37°C for 20 min. The data is from two independent experiments with each one in triplicate. The *P*-values (*P < 0.05; **P < 0.01) were determined by two-tailed unpaired *t* test. n.s., not significant. The *P*-values are 0.009 (B, 1 versus 5-mer), 0.118 (B, 1 versus 10-mer), 0.002 (B, 5 versus 10-mer), 0.003 (C, 1 versus 5-mer), 0.005 (C, 1 versus 10-mer), 0.026 (C, 5 versus 10-mer), 0.118 (D, 1 versus 5-mer), 0.002 (D, 1 versus 10-mer), and 0.010 (D, 5 versus 10-mer).

Table 2. Steady-state kinetic constants of removing 3′-PUA–OxyLys–peptide$_{10mer}$ within nicked DNA by TDP1 and APE1. a. The data is the average and standard deviation from three independent experiments

Enzyme	K_m (μM)	k_{cat} (min^{-1})	k_{cat}/K_m (μM^{-1} min^{-1})[a]
TDP1	0.34 ± 0.07	0.83 ± 0.18	2.48 ± 0.44
APE1	0.40 ± 0.06	1.68 ± 0.02	4.38 ± 0.68

sites and single-strand breaks, are produced within 1–2 helical turns of DNA, are a hallmark of γ-irradiation (90). It has been demonstrated that when two AP sites or one AP site and a single-strand break are proximally located at two DNA strands in a NCP, persistent 3′-PUA–histone DPCs within double-strand breaks were observed (16,17). In addition, if the DNA replication forks encounter the 3′-PUA–protein DPCs, double-strand breaks with the DPCs

located within 3′- and 5′-overhangs can be generated when the DPCs are in the lagging and leading strands, respectively. To determine the effect of flanking DNA structure on 3′-PUA–protein DPC removal by TDP1, APE1 and TREX1, a series of DNA substrates containing 3′-PUA–OxyLys–peptide$_{10mer}$ within a nick, blunt-end, 3′-overhang, or 5′-overhang (Figure 5A) were prepared. The free 3′-termini of the substrates used for TREX1 were blocked by phosphorylation. The completed hybridization of all substrates was verified by native PAGE (Supplementary Figure S22). We found that TDP1 removed the adduct in all substrates with similar efficiency (Figure 5B). On the contrary, APE1 strongly preferred the nick and 5′-overhangs but poorly removed the cross-link within a blunt-end or 3′-overhang (Figure 5C). Similar to TDP1, TREX1 was able to efficiently remove the adducts within all substrates but 2–3-fold less efficiently when the adduct is within the nicked DNA (Figure 5D). While TDP1 didn't have a clear preference for the overhang length, APE1 and TREX1 preferred the longer 5′-overhang and 3′-overhang, respectively. Taken together, we demonstrated that TDP1, APE1, and TREX1 have an overlapped substrate scope (nick, 5′-overhangs) but possess distinct preferences to the blunt-end and 3′-overhangs.

Effect of the opposite nucleobase on 3′-PUA–OxyLys–peptide$_{10mer}$ removal

The opposite nucleobase (if any) in the above DNA substrates is adenine (A). In theory, the one opposite to the AP site that yields the 3′-PUA–protein DPC can be either one of the four nucleobases (i.e. A, T, G and C). To determine whether TDP1, APE1 and TREX1 have any preference for the opposite nucleobase, 3′-PUA–OxyLys–peptide$_{10mer}$ was hybridized to a 42-nt complementary strand with A, T, G or C opposite to the adduct (Figure 6A). The completed hybridization was confirmed by native PAGE (Supplementary Figure S23). As shown in Figure 6B-D, both TDP1 and APE1 removed the adducts without an obvious preference to the opposite nucleobase. However, when the opposite base is a pyrimidine (T, C), the adduct removal efficiency by TREX1 is 1.3–1.5-fold higher than that when a purine base (A, G) is opposite.

TDP1, APE1 and TREX1 remove stabilized 3′-PUA–histone DPCs

Having observed that a 10-mer histone peptide conjugated to 3′-PUA can be efficiently removed by TDP1, APE1 and TREX1, we then asked whether these nucleases can directly remove the 3′-PUA–histone DPC in which a 11–13 kDa protein is conjugated to the DNA. To address this question, we prepared stabilized 3′-PUA-H2B and 3′-PUA-H4 DPCs (Figure 7A) through reductive amination (50). It should be noted that the DPCs prepared by this method are site-specific to DNA, but not for histones as the N-terminal amine or one of the histone lysine residues could react with the AP site (17). The purified 3′-PUA–histone DPCs were hybridized to a complementary strand with adenine as the opposite nucleobase and incubated with increasing concentrations of nucleases. The reaction products were ana-
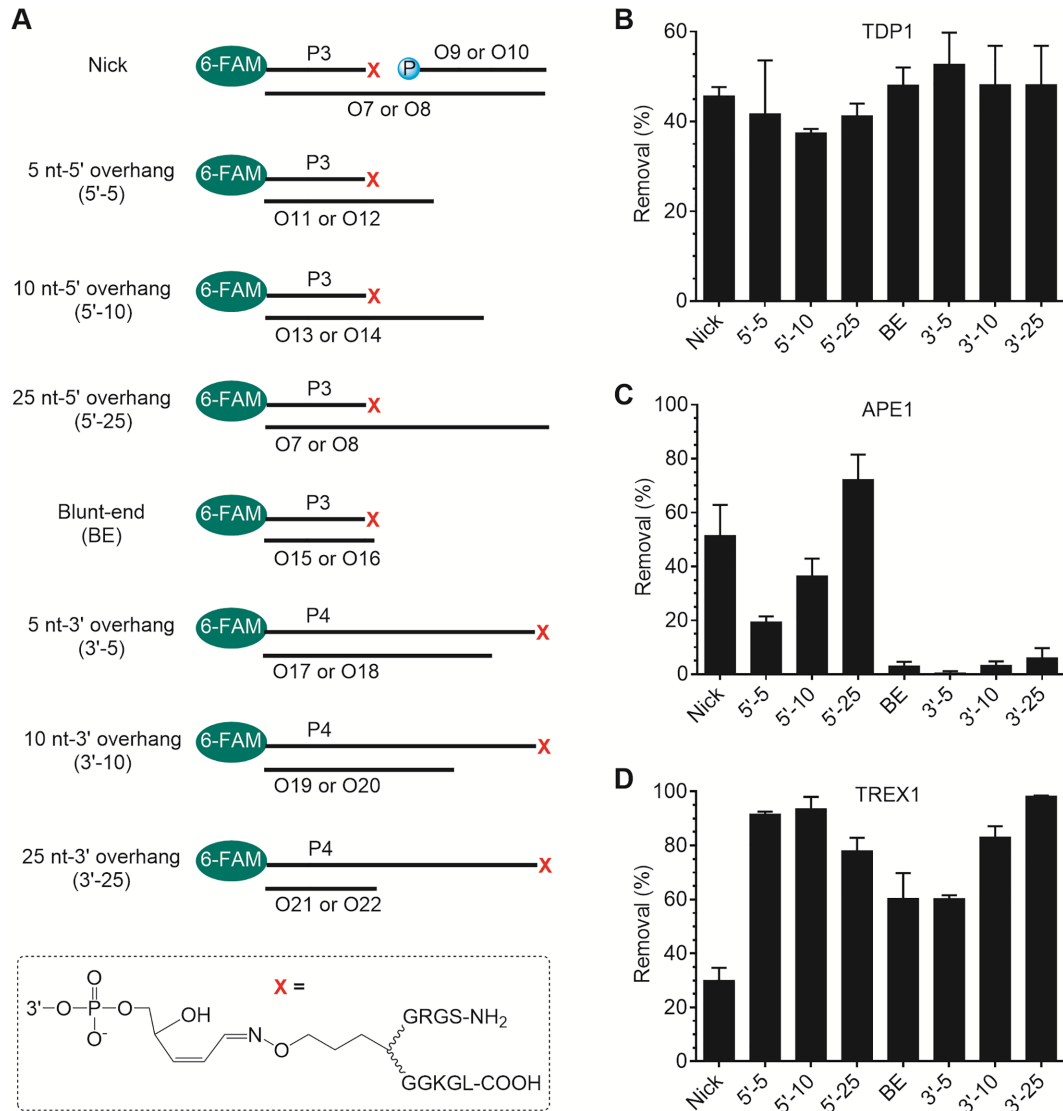
Figure 5. Flanking DNA structure effect on 3′-PUA–OxyLys–peptide$_{10mer}$ removal by TDP1, APE1 and TREX1. (**A**) Substrates containing 3′-PUA–OxyLys–peptide$_{10mer}$ with different flanking structure. (**B–D**) The plots showing the adduct removal by TDP1 (B), APE1 (C) and TREX1 (D) as a function of flanking DNA structure. The free 3′-termini used for TREX1 experiments were blocked by phosphorylation. The reactions were carried out by incubating the substrates (20 nM) at 37°C with TDP1 (50 nM, 30 min), APE1 (10 nM, 1 h) or TREX1 (2 nM, 30 min). The data is from two independent experiments with each one in triplicate.

lyzed by SDS-PAGE (Supplementary Figure S24). Notably, both 3′-PUA-H2B and 3′-PUA-H4 DPCs were removed by TDP1, APE1, and TREX1 with moderate efficiency (Figure 7B-D). Compared to 3′-PUA-H2B, 3′-PUA-H4 is a slightly better substrate possibly due to its smaller size. TDP1 and TREX1 removed the DPCs in an enzyme concentration-dependent manner and 80–90% of the DPCs were removed at the highest enzyme concentration (Figure 7B and D). However, 40–50% of the DPCs were removed by APE1 in an enzyme concentration (0–20 nM)-dependent manner but the efficiency didn't increase obviously when the concentration of APE1 increased to 50–200 nM (Figure 7C). This indicates that APE1 is only able to remove a portion of the heterogeneous 3′-PUA–histone DPCs. Taken together, these results suggest that TDP1, APE1, and TREX1 can directly remove stabilized 3′-PUA–histone DPCs. This finding

is strikingly different from other human DNA-histone DPC tolerance or repair pathways. For example, conjugating a histone to 5-formylcytosine and oxanine completely blocked the human translesion DNA synthesis and nucleotide excision repair, respectively (91,92).

Proteolysis is required for 3′-PUA–PARP1 DPC repair by TPD1, APE1, and TREX1

The formation of 3′-PUA–PARP1 DPCs has been well characterized by Wilson *et al.* *in vitro* (28). These DPCs were also observed in mammalian cells following treatment by DNA methylating agents and PARP1 inhibitors that are commonly used as anticancer drugs (28,53). Hence, it is important to understand how they are repaired. Wilson *et al.* have previously found that both TDP1 and APE1 failed
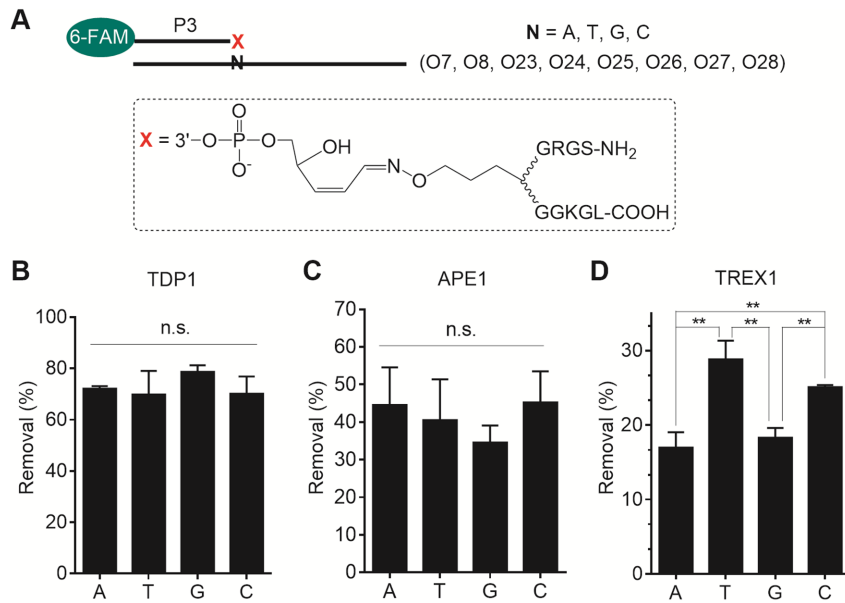
Figure 6. Effect of the opposite nucleobase on removal of 3′-PUA–OxyLys–peptide$_{10mer}$ by TDP1, APE1 and TREX1. (**A**) Substrates containing 3′-PUA–OxyLys–peptide$_{10mer}$ with different opposite nucleobases. (**B–D**) The plots showing the adduct removal by TDP1 (B), APE1 (C) and TREX1 (D). The reactions were carried out by incubating the substrate (20 nM) with TDP1 (50 nM, 30 min), APE1 (10 nM, 30 min) or TREX1 (2 nM, 15 min) at 37°C. The data is from three independent experiments. The *P*-values (*P < 0.05; **P < 0.01) were determined by two-tailed unpaired *t* test. For clarity, the difference between A and G, or T and C in panel D, which is not significant (n.s.), is not annotated. The *P*-values in panel D (TREX1) are 0.003 (A versus T), 0.398 (A versus G), 0.003 (A versus C), 0.003 (T versus G), 0.065 (T versus C) and 0.002 (G versus C).
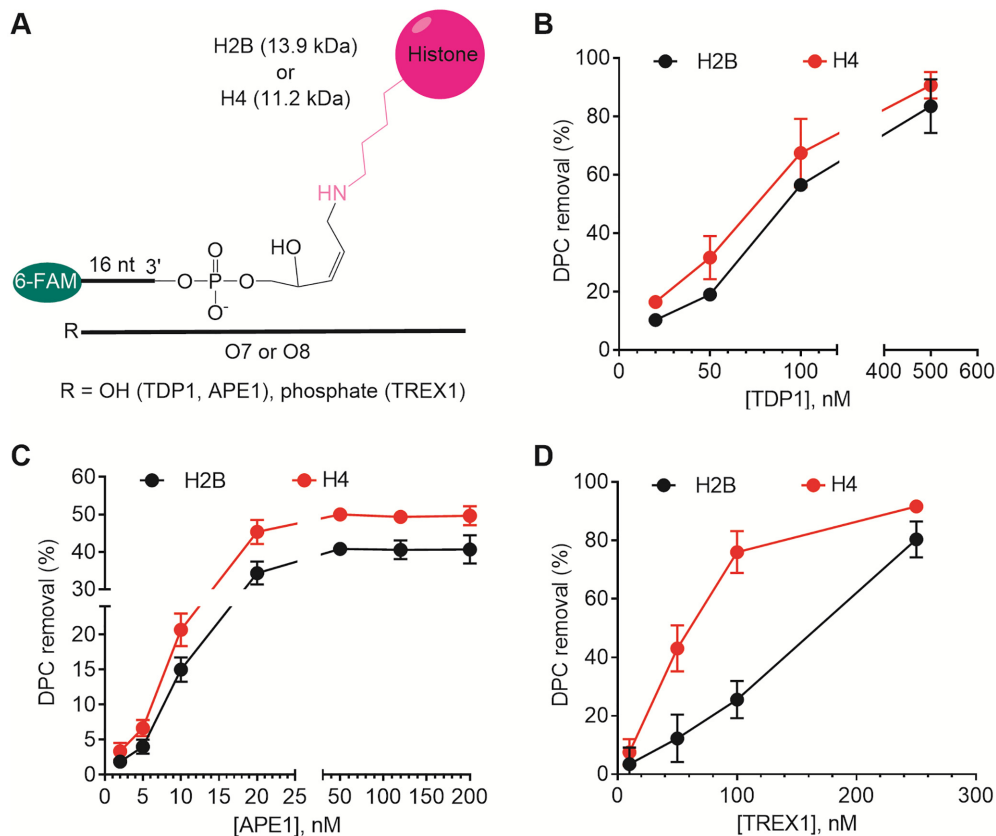

Figure 7. Removal of 3′-PUA–histone DPCs by TDP1, APE1 and TREX1. (**A**) Structure of 3′-PUA–histone DPCs prepared by reductive amination. (**B–D**) Plots showing the efficiency of 3′-PUA–histone DPC removal by TDP1 (B), APE1 (C) and TREX1 (D). The reactions were carried out by incubating the DPC substrates (60 nM) and indicated concentration of enzyme at 37°C for 60 min. The data is from three independent experiments.

to remove 3′-PUA–PARP1 DPC *in vitro* likely due to the large size (∼113 kDa) (28,53). We prepared 3′-PUA–PARP1 DPC in a similar way and also didn't observe the DPC removal by TREX1$_{1–242}$ (Supplementary Figure S25A). We ruled out the possibility that the TREX1 was inactivated under this condition as when the 3′-PUA–PARP1 DPC was prepared using 3′-OH-containing oligos, the unreacted free DNA was effectively degraded, but not the 3′-PUA–PARP1 DPC (Supplementary Figure S25B). In addition, all three nucleases failed to remove the purified 3′-PUA–PARP1 DPC (Supplementary Figure S26) under the reaction conditions where 3′-PUA–histone DPCs were effectively removed (Figure 7). All these results suggest the necessity of proteolysis for repairing a larger DPC. Indeed, recently, PARP1-DPCs have been found to be degraded by both proteasome and Spartan in cells (53,54). However, how the remaining 3′-PUA–PARP1 peptides that still prevent the DNA synthesis and strand ligation are repaired is not clear. Based on our aforementioned biochemical studies of 3′-PUA–OxyLys–peptide and 3′-PUA–histone DPC repair, we believe that proteolysis-induced 3′-PUA–PARP1 peptide cross-links will be removed by TDP1, APE1 and TREX1. To affirm this, following cross-linking PARP1 to the AP site, the reaction mixture was treated by proteinase K, which degraded the cross-linked PARP1 to a combination of 2–10 mer peptides with the predominant ones as 2–5 mer (Figure 8). The mixture containing unreacted AP site and 3′-PUA–PARP1 peptide cross-links were purified and treated by increasing concentrations of TDP1, APE1 or TREX1, and the products were analyzed by urea–PAGE (Figure 8B–D). Indeed, the 3′-PUA–PARP1 peptide adducts were removed by all three nucleases. Thus, we conclude that coupled with proteolysis, the 3′-PUA–PARP1 DPC can be repaired by TDP1, APE1 and/or TREX1 *in vitro*.

CONCLUSION

Both AP site and 3′-PUA are abundant cellular DNA lesions (2,19). Their aldehyde moieties act as electrophiles that can react with protein nucleophiles (e.g. lysine and cysteine residues) to yield various types of covalent DPCs, such as Schiff base (16,17,26,38,43,45,48,93,94), thiazolidine (34,35,37,95) or S-glycosidic bond (36) linked AP-protein adducts, and 3′-PUA–protein DPCs linked by (reduced) Schiff bases (16,17,25,28–30,50) or produced via a Michael addition reaction (32). These DPCs are either considered as new types of DNA damage or proposed to temporarily protect the lesions from error-prone repair (25,37). This study focused on addressing how 3′-PUA–protein DPCs are repaired. These DPCs are either unstable but can be long-lived, such as 3′-PUA–histone DPCs, or stable like 3′-PUA–PARP1 DPCs. They need to be removed because 3′-OH is required for DNA synthesis or strand ligation. However, how they are eradicated is not well understood partially due to the difficulties in obtaining stable, structure-defined, and physiologically relevant DPC substrates in large quantities. In this study, we developed a chemical approach for the first time to synthesize stable and site-specific 3′-PUA-peptide cross-links through bioorthogonal oxime ligation, which were used for *in vitro* reconstitu-

tion resulting in the discovery of TDP1, APE1 and TREX1 for repairing 3′-PUA-peptide adducts. This approach allowed us to make a nanomole scale of substrates to detailly characterize these novel repair pathways. Using reductive amination, we prepared stabilized 3′-PUA–histone DPCs and demonstrated that they can be directly removed by TDP1, APE1 and TREX1. We also found that larger DPCs, such as 3′-PUA–PARP1 DPC, require proteolysis prior to the repair by these nucleases. This observation is in line with the finding that PARP1-DPCs are degraded by the proteasome and Spartan in mammalian cells (53,54). This finding also supports the current DPC repair model that proteolysis is required for efficient DPC removal (24,61–67,96). Whether and how 3′-PUA–protein DPC proteolysis and eradicating 3′-PUA-peptide adducts by nucleases are integrated warrant future investigation.

Our study identified three human enzymes, TDP1, APE1 and TREX1, for repairing 3′-PUA–protein DPCs. TDP1 is a well-characterized enzyme that is dedicated to topoisomerase 1-DNA cross-link repair (72). Our finding that TDP1 removes 3′-PUA-peptide and 3′-PUA–histone DPCs revealed an additional role of TDP1 in DNA repair. Our study is the first time to report that APE1 is able to repair bulky 3′-end DNA–peptide/protein adducts. This is also the first time to reveal that TREX1 may directly contribute to DNA repair by removing 3′-PUA–peptide and 3′-PUA–protein adducts. Our *in vitro* finding is in line with the cellular observation that 1). TREX1 is upregulated and/or translocates to the nucleus in response to the treatment with DNA damage agents including ultraviolet (UV), H_2O_2, arsenite, and hydroxyurea (84,85,97); and 2). TREX1-deficient cells have reduced recovery after UV treatment, and siRNA knockdown of TREX1 sensitizes the cells to UV (84). These agents are known to induce AP sites likely resulting in enhanced 3′-PUA-peptide/protein adduct formation (3,37,98,99). The reason why TREX1 removes 3′-PUA-peptide/protein adducts, but not other 3′-obstructive lesions, needs future structural characterization. Whether other 3′-PUA-peptide adduct repair enzyme(s) exists remains elusive. If our *in vitro* observations are true in cells, why does it require multiple enzymes to eradicate 3′-PUA-peptide/protein adducts? We believe that redundant pathways could allow more rapid response and efficient repair. This has been observed for other DNA lesions, such as AP sites that can be repaired by both base excision repair and nucleotide excision repair (100). In addition, these nucleases could work complementarily to achieve the repair in a large substrate scope. Based on our findings (Figure 5), when the adduct is located at a nick or 3′-recessed ends (5′-overhangs), all three nucleases can work redundantly. However, when the cross-link is at the blunt-end or 3′-overhangs, TDP1 and TREX1, but not APE1, likely will be responsible for the repair. Moreover, these nucleases could work under different genotoxic stress conditions. For example, while APE1 is normally localized in the nucleus, TREX1 is located in the cytoplasm under normal conditions but will translocate to the nucleus in response to DNA damage induced by UV, γ-irradiation, hydroxyurea, or arsenite (84,85,97). Therefore, we envision that TREX1's DNA repair activity is activated possibly only when the DNA damage repair is overwhelmed.
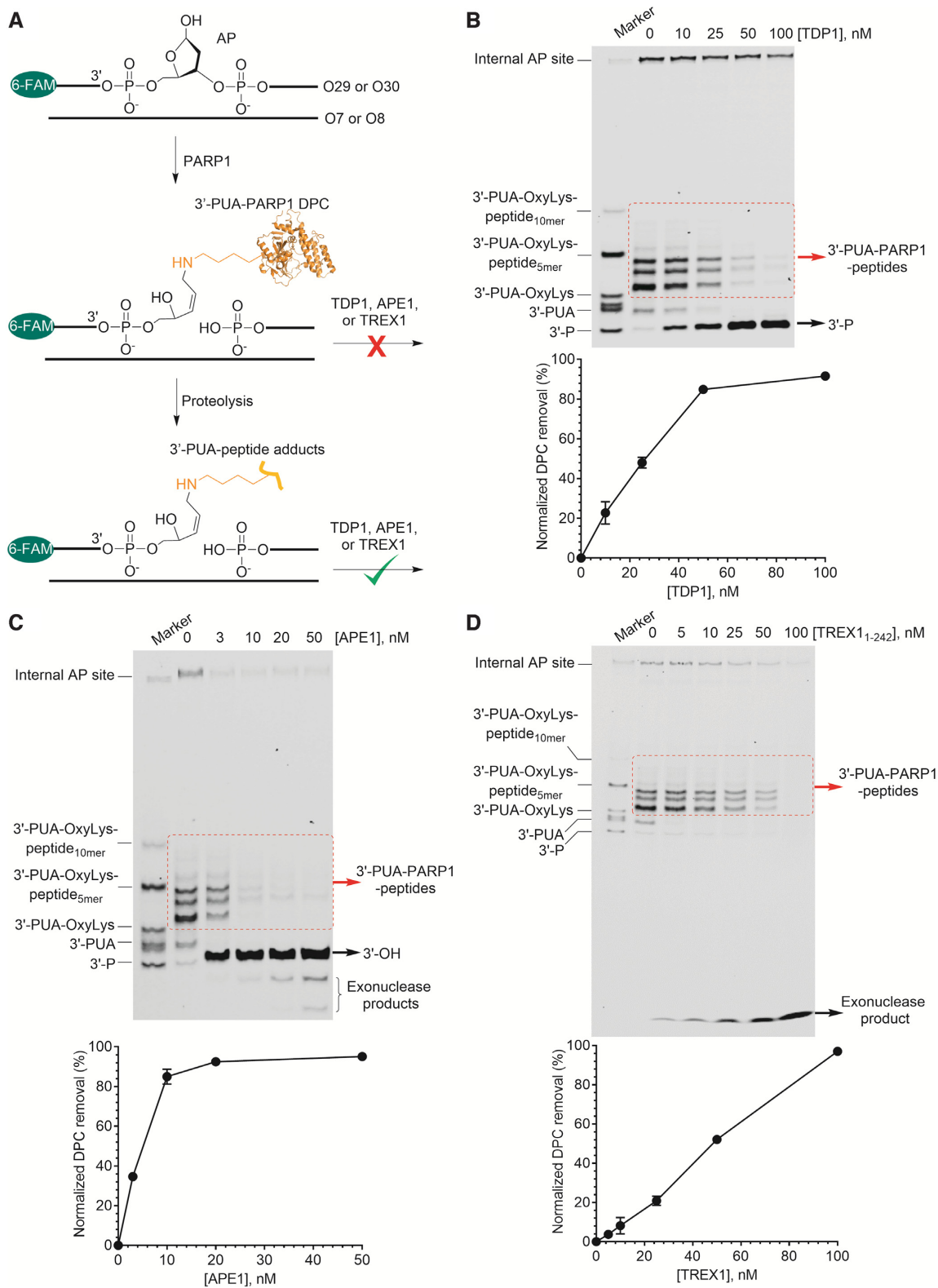
Figure 8. Repair of proteinase K-digested 3′-PUA–PARP1 DPCs by TDP1, APE1 and TREX1. (**A**) Illustration of preparing and repairing the 3′-PUA–PARP1 DPC and its proteolyzed products. (**B–D**) Representative 20% urea–PAGE gels and plots showing the repair of 3′-PUA–PARP1 peptides by TDP1 (B), APE1 (C) and TREX1 (D). The reactions were carried out by incubating the mixture of unreacted AP sites and 3′-PUA-peptide adducts (100 nM) with indicated concentrations of enzyme at 37°C for 60 min. The data is from two independent experiments. The urea–PAGE gels in B–D were scanned using the fluorescence of 6-FAM.

Our observation that APE1 repairs 3′-PUA-peptide/protein adducts is in line with Gates's recent finding that APE1 unhooks 3′-PUA–DNA interstrand cross-links (22). In both cases, APE1 incises the DNA strand at the 5′-side of the adduct. Based on our studies, we speculate that 3′-PUA–DNA interstrand cross-links can also be resolved by TDP1 and TREX1.

SUPPLEMENTARY DATA

Supplementary Data are available at NAR Online.

REFERENCES

1. Lindahl,T. (1993) Instability and decay of the primary structure of DNA. *Nature*, **362**, 709–715.
2. Atamna,H., Cheung,I. and Ames,B.N. (2000) A method for detecting abasic sites in living cells: age-dependent changes in base excision repair. *Proc. Natl. Acad. Sci. U.S.A.*, **97**, 686–691.
3. Kidane,D., Murphy,D.L. and Sweasy,J.B. (2014) Accumulation of abasic sites induces genomic instability in normal human gastric epithelial cells during helicobacter pylori infection. *Oncogenesis*, **3**, e128.
4. Higuchi,K., Katayama,T., Iwai,S., Hidaka,M., Horiuchi,T. and Maki,H. (2003) Fate of DNA replication fork encountering a single DNA lesion during oriC plasmid DNA replication in vitro. *Genes Cells*, **8**, 437–449.
5. Wang,W., Walmacq,C., Chong,J., Kashlev,M. and Wang,D. (2018) Structural basis of transcriptional stalling and bypass of abasic DNA lesion by RNA polymerase iI. *Proc. Natl. Acad. Sci. U.S.A.*, **115**, E2538–E2545.
6. Choi,J.Y., Lim,S., Kim,E.J., Jo,A. and Guengerich,F.P. (2010) Translesion synthesis across abasic lesions by human B-family and Y-family DNA polymerases α, δ, η, ι, κ, and REV1. *J. Mol. Biol.*, **404**, 34–44.
7. Boiteux,S. and Guillet,M. (2004) Abasic sites in DNA: repair and biological consequences in saccharomyces cerevisiae. *DNA Repair (Amst.)*, **3**, 1–12.
8. Piersen,C.E., McCullough,A.K. and Lloyd,R.S. (2000) AP lyases and dRPases: commonality of mechanism. *Mutat. Res.*, **459**, 43–53.
9. Hegde,M.L., Hazra,T.K. and Mitra,S. (2008) Early steps in the DNA base excision/single-strand interruption repair pathway in mammalian cells. *Cell Res.*, **18**, 27–47.
10. Male,R., Fosse,V.M. and Kleppe,K. (1982) Polyamine-induced hydrolysis of apurinic sites in DNA and nucleosomes. *Nucleic Acids Res.*, **10**, 6305–6318.
11. McHugh,P.J. and Knowland,J. (1995) Novel reagents for chemical cleavage at abasic sites and UV photoproducts in DNA. *Nucleic Acids Res.*, **23**, 1664–1670.
12. Georgakilas,A.G., Bennett,P.V. and Sutherland,B.M. (2002) High efficiency detection of bi-stranded abasic clusters in gamma-irradiated DNA by putrescine. *Nucleic Acids Res.*, **30**, 2800–2808.
13. Behmoaras,T., Toulmé,J.J. and Hélène,C. (1981) A tryptophan-containing peptide recognizes and cleaves DNA at apurinic sites. *Nature*, **292**, 858–859.
14. Pierre,J. and Laval,J. (1981) Specific nicking of DNA at apurinic sites by peptides containing aromatic residues. *J. Biol. Chem.*, **256**, 10217–10220.
15. Kurtz,A.J., Dodson,M.L. and Lloyd,R.S. (2002) Evidence for multiple imino intermediates and identification of reactive nucleophiles in peptide-catalyzed beta-elimination at abasic sites. *Biochemistry*, **41**, 7054–7064.
16. Sczepanski,J.T., Wong,R.S., McKnight,J.N., Bowman,G.D. and Greenberg,M.M. (2010) Rapid DNA–protein cross-linking and strand scission by an abasic site in a nucleosome core particle. *Proc. Natl. Acad. Sci. U.S.A.*, **107**, 22475–22480.
17. Zhou,C., Sczepanski,J.T. and Greenberg,M.M. (2012) Mechanistic studies on histone catalyzed cleavage of apyrimidinic/apurinic sites in nucleosome core particles. *J. Am. Chem. Soc.*, **134**, 16734–16741.
18. Xu,W., Boyd,R.M., Tree,M.O., Samkari,F. and Zhao,L. (2019) Mitochondrial transcription factor a promotes DNA strand cleavage at abasic sites. *Proc. Natl. Acad. Sci. U.S.A.*, **116**, 17792–17799.
19. Rahimoff,R., Kosmatchev,O., Kirchner,A., Pfaffeneder,T., Spada,F., Brantl,V., Müller,M. and Carell,T. (2017) 5-Formyl- and 5-Carboxydeoxycytidines do not cause accumulation of harmful repair intermediates in stem cells. *J. Am. Chem. Soc.*, **139**, 10359–10364.
20. Price,N.E., Johnson,K.M., Wang,J., Fekry,M.I., Wang,Y. and Gates,K.S. (2014) Interstrand DNA-DNA cross-link formation between adenine residues and abasic sites in duplex DNA. *J. Am. Chem. Soc.*, **136**, 3483–3490.
21. Yang,Z., Price,N.E., Johnson,K.M., Wang,Y. and Gates,K.S. (2017) Interstrand cross-links arising from strand breaks at true abasic sites in duplex DNA. *Nucleic Acids Res.*, **45**, 6275–6283.
22. Housh,K., Jha,J.S., Yang,Z., Haldar,T., Johnson,K.M., Yin,J., Wang,Y. and Gates,K.S. (2021) Formation and repair of an interstrand DNA cross-link arising from a common endogenous lesion. *J. Am. Chem. Soc.*, **143**, 15344–15357.
23. Tretyakova,N.Y., Groehler,A. and Ji,S. (2015) DNA-Protein cross-links: formation, structural identities, and biological outcomes. *Acc. Chem. Res.*, **48**, 1631–1644.
24. Wei,X., Peng,Y., Bryan,C. and Yang,K. (2021) Mechanisms of DNA–protein cross-link formation and repair. *Biochim. Biophys. Acta Proteins Proteom*, **1869**, 140669.
25. Nazarkina,Z.K., Khodyreva,S.N., Marsin,S., Lavrik,O.I. and Radicella,J.P. (2007) XRCC1 interactions with base excision repair DNA intermediates. *DNA Repair (Amst.)*, **6**, 254–264.
26. Ilina,E.S., Lavrik,O.I. and Khodyreva,S.N. (2008) Ku antigen interacts with abasic sites. *Biochim. Biophys. Acta*, **1784**, 1777–1785.
27. Khodyreva,S.N., Prasad,R., Ilina,E.S., Sukhanova,M.V., Kutuzov,M.M., Liu,Y., Hou,E.W., Wilson,S.H. and Lavrik,O.I. (2010) Apurinic/apyrimidinic (AP) site recognition by the 5'-dRP/AP lyase in poly(ADP-ribose) polymerase-1 (PARP-1). *Proc. Natl. Acad. Sci. U.S.A.*, **107**, 22090–22095.
28. Prasad,R., Horton,J.K., Chastain,P.D., Gassman,N.R., Freudenthal,B.D., Hou,E.W. and Wilson,S.H. (2014) Suicidal cross-linking of PARP-1 to AP site intermediates in cells undergoing base excision repair. *Nucleic Acids Res.*, **42**, 6337–6351.
29. Kutuzov,M.M., Khodyreva,S.N., Ilina,E.S., Sukhanova,M.V., Amé,J.C. and Lavrik,O.I. (2015) Interaction of PARP-2 with AP site containing DNA. *Biochimie*, **112**, 10–19.
30. Kosova,A.A., Khodyreva,S.N. and Lavrik,O.I. (2015) Glyceraldehyde-3-phosphate dehydrogenase (GAPDH) interacts with apurinic/apyrimidinic sites in DNA. *Mutat. Res.*, **779**, 46–57.
31. Quiñones,J.L., Thapar,U., Yu,K., Fang,Q., Sobol,R.W. and Demple,B. (2015) Enzyme mechanism-based, oxidative DNA–protein cross-links formed with DNA polymerase β in vivo. *Proc. Natl. Acad. Sci. U.S.A.*, **112**, 8602–8607.

32. Müller,T.A., Tobar,M.A., Perian,M.N. and Hausinger,R.P. (2017) Biochemical characterization of AP lyase and m. *Biochemistry*, **56**, 1899–1910.

33. Ahn,W.C., Aroli,S., Kim,J.H., Moon,J.H., Lee,G.S., Lee,M.H., Sang,P.B., Oh,B.H., Varshney,U. and Woo,E.J. (2019) Covalent binding of uracil DNA glycosylase UdgX to abasic DNA upon uracil excision. *Nat. Chem. Biol.*, **15**, 607–614.

34. Thompson,P.S., Amidon,K.M., Mohni,K.N., Cortez,D. and Eichman,B.F. (2019) Protection of abasic sites during DNA replication by a stable thiazolidine protein-DNA cross-link. *Nat. Struct. Mol. Biol.*, **26**, 613–618.

35. Wang,N., Bao,H., Chen,L., Liu,Y., Li,Y., Wu,B. and Huang,H. (2019) Molecular basis of abasic site sensing in single-stranded DNA by the SRAP domain of e. coli yedK. *Nucleic Acids Res.*, **47**, 10388–10399.

36. Chan,W., Ham,Y.H., Jin,L., Chan,H.W., Wong,Y.L., Chan,C.K. and Chung,P.Y. (2019) Quantification of a novel DNA-Protein cross-link product formed by reacting apurinic/apyrimidinic sites in DNA with cysteine residues in protein by liquid chromatography-tandem mass spectrometry coupled with the stable isotope-dilution method. *Anal. Chem.*, **91**, 4987–4994.

37. Mohni,K.N., Wessel,S.R., Zhao,R., Wojciechowski,A.C., Luzwick,J.W., Layden,H., Eichman,B.F., Thompson,P.S., Mehta,K.P.M. and Cortez,D. (2019) HMCES maintains genome integrity by shielding abasic sites in single-strand DNA. *Cell*, **176**, 144–153.

38. Ham,Y.H., Chan,K.K.J., Madej,D., Lam,H. and Chan,W. (2020) Proteomics study of DNA-Protein crosslinks in methylmethanesulfonate and fe. *Chem. Res. Toxicol.*, **33**, 2739–2744.

39. Khodyreva,S. and Lavrik,O. (2020) Non-canonical interaction of DNA repair proteins with intact and cleaved AP sites. *DNA Repair (Amst.)*, **90**, 102847.

40. Lebedeva,N.A., Rechkunova,N.I., Endutkin,A.V. and Lavrik,O.I. (2020) Apurinic/Apyrimidinic endonuclease 1 and Tyrosyl-DNA phosphodiesterase 1 prevent suicidal covalent DNA-Protein crosslink at apurinic/apyrimidinic site. *Front. Cell Dev. Biol.*, **8**, 617301.

41. Luger,K., Mäder,A.W., Richmond,R.K., Sargent,D.F. and Richmond,T.J. (1997) Crystal structure of the nucleosome core particle at 2.8 a resolution. *Nature*, **389**, 251–260.

42. Sczepanski,J.T., Zhou,C. and Greenberg,M.M. (2013) Nucleosome core particle-catalyzed strand scission at abasic sites. *Biochemistry*, **52**, 2157–2164.

43. Wang,R., Yang,K., Banerjee,S. and Greenberg,M.M. (2018) Rotational effects within nucleosome core particles on abasic site reactivity. *Biochemistry*, **57**, 3945–3952.

44. Yang,K. and Greenberg,M.M. (2018) Enhanced cleavage at abasic sites within clustered lesions in nucleosome core particles. *ChemBioChem*, **19**, 2061–2065.

45. Yang,K. and Greenberg,M.M. (2019) Histone tail sequences balance their role in genetic regulation and the need to protect DNA against destruction in nucleosome core particles containing abasic sites. *ChemBioChem*, **20**, 78–82.

46. Kuduvalli,P.N., Townsend,C.A. and Tullius,T.D. (1995) Cleavage by calicheamicin gamma 1I of DNA in a nucleosome formed on the 5S RNA gene of xenopus borealis. *Biochemistry*, **34**, 3899–3906.

47. Davey,G.E., Wu,B., Dong,Y., Surana,U. and Davey,C.A. (2010) DNA stretching in the nucleosome facilitates alkylation by an intercalating antitumour agent. *Nucleic. Acids. Res.*, **38**, 2081–2088.

48. Yang,K., Park,D., Tretyakova,N.Y. and Greenberg,M.M. (2018) Histone tails decrease N7-methyl-2′-deoxyguanosine depurination and yield DNA–protein cross-links in nucleosome core particles and cells. *Proc. Natl. Acad. Sci. U.S.A.*, **115**, E11212–E11220.

49. Hill,J.W., Hazra,T.K., Izumi,T. and Mitra,S. (2001) Stimulation of human 8-oxoguanine-DNA glycosylase by AP-endonuclease: potential coordination of the initial steps in base excision repair. *Nucleic Acids Res.*, **29**, 430–438.

50. Ren,M., Shang,M., Wang,H., Xi,Z. and Zhou,C. (2020) Histones participate in base excision repair of 8-oxodGuo by transiently cross-linking with active repair intermediates in nucleosome core particles. *Nucleic Acids Res.*, **49**, 257–268.

51. Quiñones,J.L., Thapar,U., Wilson,S.H., Ramsden,D.A. and Demple,B. (2020) Oxidative DNA–protein cross-links formed in mammalian cells by abasic site lyases involved in DNA repair. *DNA Repair (Amst.)*, **87**, 102773.

52. Ray Chaudhuri,A. and Nussenzweig,A. (2017) The multifaceted roles of PARP1 in DNA repair and chromatin remodelling. *Nat. Rev. Mol. Cell Biol.*, **18**, 610–621.

53. Prasad,R., Horton,J.K., Dai,D.P. and Wilson,S.H. (2019) Repair pathway for PARP-1 DNA–protein crosslinks. *DNA Repair (Amst.)*, **73**, 71–77.

54. Saha,L.K., Murai,Y., Saha,S., Jo,U., Tsuda,M., Takeda,S. and Pommier,Y. (2021) Replication-dependent cytotoxicity and Spartan-mediated repair of trapped PARP1-DNA complexes. *Nucleic Acids Res.*, **49**, 10493–10506.

55. Stanley,M. and Virdee,S. (2016) Genetically directed production of recombinant, isosteric and nonhydrolysable ubiquitin conjugates. *ChemBioChem*, **17**, 1472–1480.

56. Pujari,S.S., Zhang,Y., Ji,S., Distefano,M.D. and Tretyakova,N.Y. (2018) Site-specific cross-linking of proteins to DNA via a new bioorthogonal approach employing oxime ligation. *Chem. Commun. (Camb.)*, **54**, 6296–6299.

57. Hemphill,W.O. and Perrino,F.W. (2019) Measuring TREX1 and TREX2 exonuclease activities. *Methods Enzymol.*, **625**, 109–133.

58. Langelier,M.F., Steffen,J.D., Riccio,A.A., McCauley,M. and Pascal,J.M. (2017) Purification of DNA damage-dependent PARPs from e. coli for structural and biochemical analysis. *Methods Mol. Biol.*, **1608**, 431–444.

59. Ji,S., Shao,H., Han,Q., Seiler,C.L. and Tretyakova,N.Y. (2017) Reversible DNA-protein cross-linking at epigenetic DNA marks. *Angew. Chem. Int. Ed Engl.*, **56**, 14130–14134.

60. Zou Guangrong,L.C., Weiwu,Z., Wei,Y., Kaiyuan,Z., Yalun,X., Cong,C. and Xiang,Z. (2020). Regulable DNA–Protein interactions in vitro and vivo at epigenetic DNA marks. *Chinese Chem. Soc.*, **2**, 54–63.

61. Stingele,J. and Jentsch,S. (2015) DNA–protein crosslink repair. *Nat. Rev. Mol. Cell Biol.*, **16**, 455–460.

62. Stingele,J., Bellelli,R. and Boulton,S.J. (2017) Mechanisms of DNA–protein crosslink repair. *Nat. Rev. Mol. Cell Biol.*, **18**, 563–573.

63. Klages-Mundt,N.L. and Li,L. (2017) Formation and repair of DNA–protein crosslink damage. *Sci China Life Sci*, **60**, 1065–1076.

64. Kühbacher,U. and Duxin,J.P. (2020) How to fix DNA–protein crosslinks. *DNA Repair (Amst.)*, **94**, 102924.

65. Kojima,Y. and Machida,Y.J. (2020) DNA–protein crosslinks from environmental exposure: mechanisms of formation and repair. *Environ. Mol. Mutagen.*, **61**, 716–729.

66. Ruggiano,A. and Ramadan,K. (2021) The trinity of SPRTN protease regulation. *Trends Biochem. Sci*, **46**, 2–4.

67. Ruggiano,A. and Ramadan,K. (2021) DNA–protein crosslink proteases in genome stability. *Commun. Biol.*, **4**, 11.

68. Darwanto,A., Farrel,A., Rogstad,D.K. and Sowers,L.C. (2009) Characterization of DNA glycosylase activity by matrix-assisted laser desorption/ionization time-of-flight mass spectrometry. *Anal. Biochem.*, **394**, 13–23.

69. Alexeeva,M., Moen,M.N., Grøsvik,K., Tesfahun,A.N., Xu,X.M., Muruzábal-Lecumberri,I., Olsen,K.M., Rasmussen,A., Ruoff,P., Kirpekar,F. *et al.* (2019) Excision of uracil from DNA by hSMUG1 includes strand incision and processing. *Nucleic Acids Res.*, **47**, 779–793.

70. Mazumder,A., Gerlt,J.A., Absalon,M.J., Stubbe,J., Cunningham,R.P., Withka,J. and Bolton,P.H. (1991) Stereochemical studies of the beta-elimination reactions at aldehydic abasic sites in DNA: endonuclease III from *Escherichia coli*, sodium hydroxide, and lys-trp-lys. *Biochemistry*, **30**, 1119–1126.

71. Sugiyama,H., Fujiwara,T., Ura,A., Tashiro,T., Yamamoto,K., Kawanishi,S. and Saito,I. (1994) Chemistry of thermal degradation of abasic sites in DNA. Mechanistic investigation on thermal DNA strand cleavage of alkylated DNA. *Chem. Res. Toxicol.*, **7**, 673–683.

72. Interthal,H., Chen,H.J. and Champoux,J.J. (2005) Human tdp1 cleaves a broad spectrum of substrates, including phosphoamide linkages. *J. Biol. Chem.*, **280**, 36518–36528.

73. Murai,J., Huang,S.Y., Das,B.B., Dexheimer,T.S., Takeda,S. and Pommier,Y. (2012) Tyrosyl-DNA phosphodiesterase 1 (TDP1) repairs DNA damage induced by topoisomerases i and II and base alkylation in vertebrate cells. *J. Biol. Chem.*, **287**, 12848–12857.

74. Whitaker,A.M. and Freudenthal,B.D. (2018) APE1: a skilled nucleic acid surgeon. *DNA Repair (Amst.)*, **71**, 93–100.

75. Rosa,S., Fortini,P., Karran,P., Bignami,M. and Dogliotti,E. (1991) Processing in vitro of an abasic site reacted with methoxyamine: a new assay for the detection of abasic sites formed in vivo. *Nucleic Acids Res.*, **19**, 5569–5574.

76. Prasad,R., Liu,Y., Deterding,L.J., Poltoratsky,V.P., Kedar,P.S., Horton,J.K., Kanno,S., Asagoshi,K., Hou,E.W., Khodyreva,S.N. *et al.* (2007) HMGB1 is a cofactor in mammalian base excision repair. *Mol. Cell*, **27**, 829–841.

77. Mol,C.D., Izumi,T., Mitra,S. and Tainer,J.A. (2000) DNA-bound structures and mutants reveal abasic DNA binding by APE1 and DNA repair coordination [corrected]. *Nature*, **403**, 451–456.

78. Freudenthal,B.D., Beard,W.A., Cuneo,M.J., Dyrkheeva,N.S. and Wilson,S.H. (2015) Capturing snapshots of APE1 processing DNA damage. *Nat. Struct. Mol. Biol.*, **22**, 924–931.

79. Whitaker,A.M., Flynn,T.S. and Freudenthal,B.D. (2018) Molecular snapshots of APE1 proofreading mismatches and removing DNA damage. *Nat. Commun.*, **9**, 399.

80. Stetson,D.B., Ko,J.S., Heidmann,T. and Medzhitov,R. (2008) Trex1 prevents cell-intrinsic initiation of autoimmunity. *Cell*, **134**, 587–598.

81. Crow,Y.J., Hayward,B.E., Parmar,R., Robins,P., Leitch,A., Ali,M., Black,D.N., van Bokhoven,H., Brunner,H.G., Hamel,B.C. *et al.* (2006) Mutations in the gene encoding the 3'-5' DNA exonuclease TREX1 cause aicardi-goutières syndrome at the AGS1 locus. *Nat. Genet.*, **38**, 917–920.

82. Rice,G., Newman,W.G., Dean,J., Patrick,T., Parmar,R., Flintoff,K., Robins,P., Harvey,S., Hollis,T., O'Hara,A. *et al.* (2007) Heterozygous mutations in TREX1 cause familial chilblain lupus and dominant aicardi-goutieres syndrome. *Am. J. Hum. Genet.*, **80**, 811–815.

83. Lehtinen,D.A., Harvey,S., Mulcahy,M.J., Hollis,T. and Perrino,F.W. (2008) The TREX1 double-stranded DNA degradation activity is defective in dominant mutations associated with autoimmune disease. *J. Biol. Chem.*, **283**, 31649–31656.

84. Christmann,M., Tomicic,M.T., Aasland,D., Berdelle,N. and Kaina,B. (2010) Three prime exonuclease i (TREX1) is fos/ap-1 regulated by genotoxic stress and protects against ultraviolet light and benzo(a)pyrene-induced DNA damage. *Nucleic Acids Res.*, **38**, 6418–6432.

85. Miyazaki,T., Kim,Y.S., Yoon,J., Wang,H., Suzuki,T. and Morse,H.C. (2014) The 3'-5' DNA exonuclease TREX1 directly interacts with poly(ADP-ribose) polymerase-1 (PARP1) during the DNA damage response. *J. Biol. Chem.*, **289**, 32548–32558.

86. Harrigan,J.A., Fan,J., Momand,J., Perrino,F.W., Bohr,V.A. and Wilson,D.M. (2007) WRN exonuclease activity is blocked by DNA termini harboring 3' obstructive groups. *Mech. Ageing Dev.*, **128**, 259–266.

87. Simpson,S.R., Hemphill,W.O., Hudson,T. and Perrino,F.W. (2020) TREX1 - apex predator of cytosolic DNA metabolism. *DNA Repair (Amst.)*, **94**, 102894.

88. Raymond,A.C., Staker,B.L. and Burgin,A.B. (2005) Substrate specificity of tyrosyl-DNA phosphodiesterase i (Tdp1). *J. Biol. Chem.*, **280**, 22029–22035.

89. Shevelev,I.V. and Hübscher,U. (2002) The 3' 5' exonucleases. *Nat. Rev. Mol. Cell Biol.*, **3**, 364–376.

90. Goodhead,D.T. (1994) Initial events in the cellular effects of ionizing radiations: clustered damage in DNA. *Int. J. Radiat. Biol.*, **65**, 7–17.

91. Pujari,S.S., Wu,M., Thomforde,J., Wang,Z.A., Chao,C., Olson,N., Erber,L., Pomerantz,W.C.K., Cole,P. and Tretyakova,N.Y. (2021) Site-Specific 5-Formyl cytosine mediated DNA-Histone cross-links: synthesis and polymerase bypass by human DNA polymerase η. *Angew. Chem. Int. Ed Engl.*, **60**, 26489–26494.

92. Nakano,T., Katafuchi,A., Matsubara,M., Terato,H., Tsuboi,T., Masuda,T., Tatsumoto,T., Pack,S.P., Makino,K., Croteau,D.L. *et al.* (2009) Homologous recombination but not nucleotide excision repair plays a pivotal role in tolerance of DNA–protein cross-links in mammalian cells. *J. Biol. Chem.*, **284**, 27065–27076.

93. Yang,K., Sun,H., Lowder,L., Varadarajan,S. and Greenberg,M.M. (2019) Reactivity of N3-methyl-2'-deoxyadenosine in nucleosome core particles. *Chem. Res. Toxicol.*, **32**, 2118–2124.

94. Yang,K., Prasse,C. and Greenberg,M.M. (2019) Effect of histone lysine methylation on DNA lesion reactivity in nucleosome core particles. *Chem. Res. Toxicol.*, **32**, 910–916.

95. Halabelian,L., Ravichandran,M., Li,Y., Zeng,H., Rao,A., Aravind,L. and Arrowsmith,C.H. (2019) Structural basis of HMCES interactions with abasic DNA and multivalent substrate recognition. *Nat. Struct. Mol. Biol.*, **26**, 607–612.

96. Sun,Y., Saha,S., Wang,W., Saha,L.K., Huang,S.N. and Pommier,Y. (2020) Excision repair of topoisomerase DNA–protein crosslinks (TOP-DPC). *DNA Repair (Amst.)*, **89**, 102837.

97. Yang,Y.G., Lindahl,T. and Barnes,D.E. (2007) Trex1 exonuclease degrades ssDNA to prevent chronic checkpoint activation and autoimmune disease. *Cell*, **131**, 873–886.

98. Fung,H., Liu,P. and Demple,B. (2007) ATF4-dependent oxidative induction of the DNA repair enzyme ape1 counteracts arsenite cytotoxicity and suppresses arsenite-mediated mutagenesis. *Mol. Cell. Biol.*, **27**, 8834–8847.

99. Sakano,K., Oikawa,S., Hasegawa,K. and Kawanishi,S. (2001) Hydroxyurea induces site-specific DNA damage via formation of hydrogen peroxide and nitric oxide. *Jpn. J. Cancer Res.*, **92**, 1166–1174.

100. Kitsera,N., Rodriguez-Alvarez,M., Emmert,S., Carell,T. and Khobta,A. (2019) Nucleotide excision repair of abasic DNA lesions. *Nucleic Acids Res.*, **47**, 8537–8547.